

# Generative Quantile Regression with Variability Penalty

Shijie Wang<sup>1</sup>, Minsuk Shin<sup>2</sup>, and Ray Bai<sup>1</sup>

<sup>1</sup>Department of Statistics, University of South Carolina, Columbia, SC 29208

E-mails: shijiew@email.sc.edu, rbai@mailbox.sc.edu

<sup>2</sup>Gauss Labs, Palo Alto, CA 94301

## Abstract

Quantile regression and conditional density estimation can reveal structure that is missed by mean regression, such as multimodality and skewness. In this paper, we introduce a deep learning generative model for joint quantile estimation called Penalized Generative Quantile Regression (PGQR). Our approach simultaneously generates samples from many random quantile levels, allowing us to infer the conditional distribution of a response variable given a set of covariates. Our method employs a novel variability penalty to avoid the problem of vanishing variability, or memorization, in deep generative models. Further, we introduce a new family of partial monotonic neural networks (PMNN) to circumvent the problem of crossing quantile curves. A major benefit of PGQR is that it can be fit using a single optimization, thus bypassing the need to repeatedly train the model at multiple quantile levels or use computationally expensive cross-validation to tune the penalty parameter. We illustrate the efficacy of PGQR through extensive simulation studies and analysis of real datasets. Code to implement our method is available at <https://github.com/shijiew97/PGQR>.

*Keywords:* conditional quantile, deep generative model, generative learning, joint quantile model, neural networks, nonparametric quantile regression

## 1 Introduction

Quantile regression is a popular alternative to classical mean regression (Koenker and Bassett Jr, 1982). For a response variable  $Y \in \mathbb{R}$  and covariates  $\mathbf{X} = (X_1, X_2, \dots, X_p)^\top \in \mathbb{R}^p$ , we define the  $\tau$ -th conditional quantile,  $\tau \in (0, 1)$ , as the  $\tau$ -th quantile of the conditional distribution of  $Y$  given  $\mathbf{X}$ , i.e.

$$Q_{Y|\mathbf{X}}(\tau) = \inf\{y : F_{Y|\mathbf{X}}(y) \geq \tau\}, \quad (1)$$

where  $F_{Y|\mathbf{X}}$  is the conditional cumulative distribution function of  $Y$  given  $\mathbf{X}$ . For a fixed quantile level  $\tau \in (0, 1)$ , linear quantile regression aims to model (1) as a linear combination of  $\mathbf{X}$ , i.e.

$Q_{Y|\mathbf{X}}(\tau) = \mathbf{X}^\top \boldsymbol{\beta}_\tau$ . Linear quantile regression is less sensitive to outliers than least squares regression and is more robust when the assumption of iid Gaussian residual errors is violated (Koenker and Hallock, 2001; Koenker et al., 2017). Thus, it is widely used for modeling heterogeneous data and heterogeneous covariate-response associations.

Numerous extensions and variants of quantile regression have been proposed. In order to reveal complex nonlinear structures, *nonparametric* quantile regression is frequently considered (Chaudhuri and Loh, 2002; Li et al., 2021; Koenker et al., 1994). For some function class  $\mathcal{F}$ , nonparametric quantile regression aims to estimate  $f(\mathbf{X}, \tau) \in \mathcal{F}$  for  $Q_{Y|\mathbf{X}}(\tau) = f(\mathbf{X}, \tau)$  at a given quantile level  $\tau$ . Many existing nonparametric quantile methods are based on either kernel smoothing or basis expansions. While quantile regression has traditionally focused on estimating the conditional quantile function at a single  $\tau$ -th quantile level, *composite* (or *joint*) quantile regression aims to estimate multiple quantile levels *simultaneously* for a set of  $K \geq 2$  quantiles  $\{\tau_1, \tau_2, \dots, \tau_K\}$ . Some nonparametric methods for composite quantile regression are proposed in Zou and Yuan (2008), Jiang et al. (2012b), Jiang et al. (2012a), and Xu et al. (2017).

Despite its flexibility, nonparametric quantile regression carries the risk that the estimated curves at different quantile levels might *cross* each other. For instance, the estimate of the 95th conditional quantile of  $Y_i$  given some covariates  $\mathbf{X}_i$  might be smaller than the estimate of the 90th conditional quantile. This is known as the *crossing quantile* phenomenon. The left two panels of Figure 4 illustrate this crossing problem. When quantile curves cross each other, the quantile estimates violate the laws of probability and are no longer reasonable. To tackle this issue, many approaches have been proposed, such as constraining the model space (Takeuchi et al., 2006; Sangnier et al., 2016; Moon et al., 2021) or the model parameters (Meinshausen, 2006; Cannon, 2018).

Recently in the area of deep learning, neural networks have also been applied to nonparametric quantile regression. Taylor (2000) used feedforward neural networks (FNNs) to estimate conditional quantiles. Takeuchi et al. (2006) considered support vector machines in combination with quantile regression. Neural networks have also been used for composite quantile regression by Xu et al. (2017) and Jin and Zhao (2021). Existing neural network-based approaches for joint quantile estimation are restricted at a prespecified quantile set. If only several quantiles (e.g. the interquartiles  $\tau \in \{0.25, 0.5, 0.75\}$ ) are of interest, then these methods are adequate to produce desirable

inference. Otherwise, one typically has to refit the model at new quantiles *or* specify a large enough quantile candidate set in order to infer the full conditional density  $p(Y | \mathbf{X})$ . Dabney et al. (2018) introduced the implicit quantile network (IQN), which takes a grid of quantile levels as inputs and approximates the conditional density at *any* quantile level (not just the given inputs). However, IQN cannot guarantee that quantile functions at different levels do not cross each other.

Composite quantile regression is closely related to the problem of *conditional density estimation* (CDE) of  $p(Y | \mathbf{X})$ . Apart from traditional CDE methods that estimate the unknown probability density curve (Izbicki and Lee, 2017; Pospisil and Lee, 2019), several deep *generative* approaches besides IQN have also been proposed. Zhou et al. (2022) introduced the generative conditional distribution sampler (GCDS), while Liu et al. (2021) introduced the Wasserstein generative conditional sampler (WGCS) for CDE. GCDS and WGCS employ the idea of generative adversarial networks (GANs) (Goodfellow et al., 2014) to *generate samples* from the conditional distribution  $p(Y | \mathbf{X})$ . In these deep generative models, random noise inputs are used to learn and generate samples from the target distribution. However, a well-known problem with deep generative networks is that the generator may simply memorize the training samples instead of generalizing to new test data (Arpit et al., 2017; van den Burg and Williams, 2021). When *memorization* occurs, the random noise variable no longer reflects any variability, and the predicted density  $p(Y | \mathbf{X})$  approaches a point mass. We refer to this phenomenon as *vanishing variability*.

To achieve the goal of joint quantile estimation as well as conditional density estimation, we propose a new deep generative approach called penalized generative quantile regression (PGQR). PGQR employs a novel variability penalty to avoid vanishing variability. Although introduced in the context of joint quantile regression, we believe that our penalty formulation is broadly applicable to other deep generative models that may suffer from memorization. We further guarantee the monotonicity (i.e. non-crossing) of the estimated quantile functions from PGQR by designing a *new* family of partial monotonic neural networks (PMNNs). The PMNN architecture ensures partial monotonicity with respect to quantile inputs, while retaining the expressiveness of neural networks.

The performance of PGQR depends crucially on carefully choosing a hyperparameter  $\lambda$ , which controls the amount of regularization by our variability penalty. However, common tuning procedures such as cross-validation are impractical for deep learning, since this would involve repetitive

evaluations of the network for different choices of  $\lambda$  and different training sets. Inspired by the generative idea from Shin et al. (2022), we construct our deep generative network in such a way that  $\lambda$  is included as an additional random input. This way, only a *single* optimization is needed to learn the neural network parameters, and then it is effortless to generate samples from a set of candidate values for  $\lambda$ . Finally, we introduce a criterion for selecting the optimal choice of  $\lambda$  which we use to generate the final desired samples from multiple quantiles of  $p(Y | \mathbf{X})$  simultaneously.

Our main contributions can be summarized as follows:

1. We propose a deep generative approach for composite quantile regression and conditional density estimation called *penalized generative quantile regression*. PGQR simultaneously generates samples from *multiple* random quantile levels, thus precluding the need to refit the model at different quantiles.
2. We introduce a novel variability penalty to avoid the vanishing variability phenomenon in deep generative models and apply this regularization technique to PGQR.
3. We construct a new family of partial monotonic neural networks (PMNNs) to circumvent the problem of crossing quantile curves.
4. To facilitate scalable computation for PGQR and bypass computationally expensive cross-validation for tuning the penalty parameter, we devise a strategy that allows PGQR to be implemented using only a *single* optimization.

The rest of the article is structured as follows. Section 2 motivates our PGQR framework with a real data application on body composition and strength in older adults. Section 3 introduces the generative quantile regression framework and our variability penalty. In Section 4, we introduce the PMNN family for preventing quantile curves from crossing each other. Section 5 discusses scalable computation for PGQR, namely how to tune the variability penalty parameter with only single-model training. In Section 6, we demonstrate the utility of PGQR through simulation studies and analyses of additional real datasets. Section 7 concludes the paper with some discussion and directions for future research.

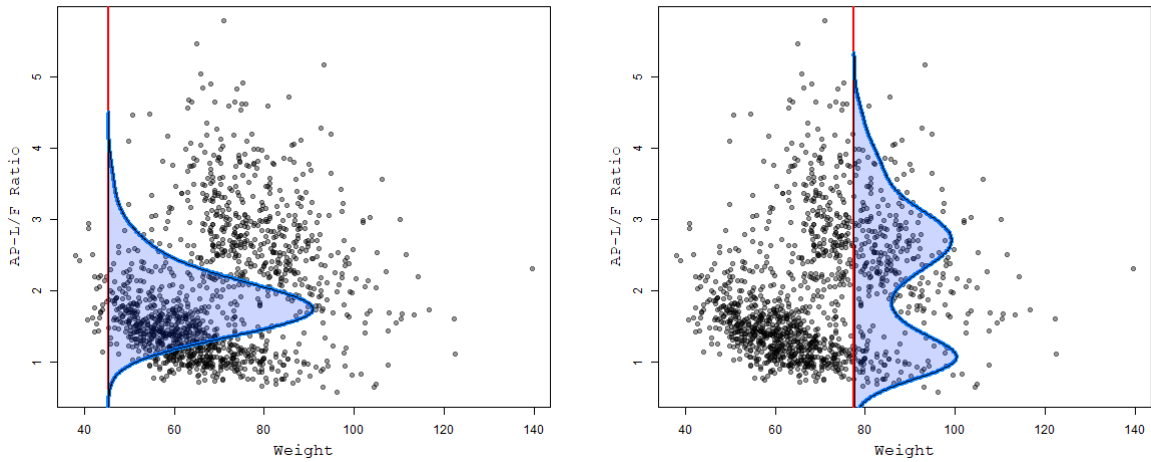


Figure 1: Using PGQR to model the conditional density of AP-L/F ratio given weight in older adults. Left panel: Weight = 45.4 kg, Right panel: Weight = 77.5 kg.

## 2 Motivating Application: Discovering Subpopulations

As discussed in Section 1, we aim to generate samples from the conditional quantiles  $Q_{Y|\mathbf{X}}(\tau)$  of  $p(Y | \mathbf{X})$  at different quantile levels  $\tau \in (0, 1)$ . An automatic byproduct of joint *nonparametric* quantile regression (as opposed to linear quantile regression) is that if the conditional quantiles  $Q_{Y|\mathbf{X}}(\tau)$  are estimated well for a large number of quantiles, then we can also infer the *entire* conditional distribution for  $Y$  given  $\mathbf{X}$ .

To motivate our methodology, we apply the proposed PGQR method (introduced in Section 3) to a dataset on body composition and strength in older adults (RoyChoudhury and Xu, 2020). The data was collected over a period of 12 years for 1466 subjects as part of the Rancho Bernardo Study (RBS), a longitudinal observational cohort study. We are interested in modeling the appendicular lean/fat (AP-L/F) ratio, i.e.

$$\text{AP-L/F Ratio} = \frac{\text{Weight on legs and arms}}{\text{Fat weight}},$$

as a function of weight (kg). Accurately predicting the AP-L/F ratio is of practical clinical interest, since the AP-L/F ratio provides information about limb tissue quality and is used to diagnose sarcopenia (age-related, involuntary loss of skeletal muscle mass and strength) in adults over the age of 30 (Evans, 2010; Scafoglieri et al., 2017).

Figure 1 plots the approximated conditional density of AP-L/F ratio given weight of 45.4 kg (left panel) and 77.5 kg (right panel) under the PGQR model. We see evidence of data heterogeneity (actually, depending on an unobserved factor of gender), as the estimated conditional density is unimodal when the weight of older adults is 45.4 kg but *bimodal* when the weight of older adults is 77.5 kg. In short, our method *discovers* the presence of two heterogeneous subpopulations of adults that weigh around 78 kg. In contrast, mean regression (e.g. simple linear regression or nonparametric mean regression) of AP-L/F ratio given weight might obscure the presence of two modes and miss the fact that weight affects AP-L/F ratio differently for these two clusters of adults.

### 3 Penalized Generative Quantile Regression

#### 3.1 Generative Quantile Regression

Before introducing PGQR, we first introduce our framework for generative quantile regression (without variability penalty). Given  $n$  training samples  $(\mathbf{X}_1, Y_1), (\mathbf{X}_2, Y_2), \dots, (\mathbf{X}_n, Y_n)$  and quantile level  $\tau \in (0, 1)$ , nonparametric quantile regression minimizes the empirical quantile loss,

$$\operatorname{argmin}_{f \in \mathcal{F}} \frac{1}{n} \sum_{i=1}^n \rho_{\tau}(Y_i - f(\mathbf{X}_i, \tau)), \quad (2)$$

where  $\rho_{\tau}(u) = u(\tau - I(u < 0))$  is the check function, and  $\mathcal{F}$  is a function class such as a reproducing kernel Hilbert space or a family of neural networks. Neural networks are a particularly attractive way to model the quantile function  $f(\mathbf{X}, \tau)$  in (2), because they are universal approximators for any Lebesgue integrable function (Lu et al., 2017).

In this paper, we choose to model the quantile function in (2) using deep neural networks (DNNs). We define a DNN as a neural network with at least two hidden layers and a fairly large number of nodes. We refer to Emmert-Streib et al. (2020) for a comprehensive review of DNNs. Despite the universal approximation properties of DNNs, we must *also* take care to ensure that our estimated quantile functions do *not* cross each other. Therefore, we have to consider a wide enough *monotonic* function class  $\mathcal{G}^m$  to cover the true  $Q_{Y|\mathbf{X}}(\cdot)$ . We formally introduce this class  $\mathcal{G}^m$  in Section 4.

Let  $G$  denote the constructed DNN, which is defined as a feature map function  $\{G \in \mathcal{G}^m :$

$\mathbb{R}^{p+1} \mapsto \mathbb{R}^1$  that takes  $(\mathbf{X}_i, \tau)$  as input and generates the conditional quantile for  $Y_i$  given  $\mathbf{X}_i$  at level  $\tau$  as output. We refer to this generative framework as *Generative Quantile Regression* (GQR). The optimization problem for GQR is

$$\hat{G} = \operatorname{argmin}_{G \in \mathcal{G}^m} \frac{1}{n} \sum_{i=1}^n \mathbb{E}_\tau \{ \rho_\tau(Y_i - G(\mathbf{X}_i, \tau)) \}, \quad (3)$$

where  $\hat{G}$  denotes the estimated quantile function with optimized parameters (i.e. the weights and biases) of the DNN. Note that optimizing the integrative loss  $\mathbb{E}_\tau \{ \cdot \}$  over  $\tau$  in (3) is justified by Proposition 3.1 introduced in the next section (i.e. we set  $\lambda = 0$  in Proposition 3.1).

In order to solve (3), we can use stochastic gradient descent (SGD) with mini-batching (Emmert-Streib et al., 2020). For each mini-batch evaluation,  $\mathbf{X}_i$  is paired with a quantile level  $\tau$  sampled from  $\text{Uniform}(0, 1)$ . Consequently, if there are  $M$  mini-batches, the expectation in (3) can be approximated by a Monte Carlo average of the random  $\tau$ 's, i.e. we approximate  $\mathbb{E}_\tau \{ \rho_\tau(Y_i - G(\mathbf{X}_i, \tau)) \}$  with  $M^{-1} \sum_{k=1}^M \{ \rho_{\tau_k}(Y_i - G(\mathbf{X}_i, \tau_k)) \}$ . Once we have solved (3), it is straightforward to use  $\hat{G}$  to generate *new* samples  $\hat{G}(\mathbf{X}, \xi_k), k = 1, 2, \dots, b$ , at various quantile levels  $\boldsymbol{\xi} = \{\xi_1, \xi_2, \dots, \xi_b\}$ , where the  $\xi$ 's are random  $\text{Uniform}(0, 1)$  noise inputs. Provided that  $b$  is large enough, the generated samples at  $\boldsymbol{\xi} \in (0, 1)^b$  can be used to reconstruct the full conditional density  $p(Y | \mathbf{X})$ .

As discussed in Section 1, there are several other deep generative models (Zhou et al., 2022; Liu et al., 2021) for generating samples from the underlying conditional distribution. These generative approaches also take random noise  $z$  as an input (typically  $z \sim \mathcal{N}(0, 1)$ ) to reflect variability, but there is no specific statistical meaning for  $z$ . In contrast, the random noise  $\tau$  in GQR (3) has a clear interpretation as a quantile level  $\tau \in (0, 1)$ . Although GQR and these other deep generative approaches are promising approaches for conditional sampling, these methods are all unfortunately prone to memorization of the training data. When this occurs, the random noise does not generate *any* variability. To remedy this, we now introduce our *variability penalty* in conjunction with our GQR loss function (3).

## 3.2 Variability Penalty for GQR

When a DNN is too overparameterized to capture the underlying structure in the training data, the random noise in DNN is likely to reflect no variability, no matter what value it inputs. We refer

this phenomenon as *vanishing variability*, and it is a common problem in deep generative models (Arpit et al., 2017; Arora et al., 2017; van den Burg and Williams, 2021). To be more specific, let  $G(\cdot, z)$  be the generator function constructed by a DNN, where  $z$  is a random noise variable following some reference distribution such as a standard Gaussian or a standard uniform. The vanishing variability phenomenon occurs when

$$\widehat{G}(\mathbf{X}_i, z) = Y_i, \quad i = 1, \dots, n. \quad (4)$$

In other words, there is no variability when inputting different random noise  $z$ , generating almost surely a discrete point mass at the training data. Additionally, given a *new* feature vector  $\mathbf{X}_{\text{new}}$ ,  $G(\mathbf{X}_{\text{new}}, z)$  can only generate one novel sample from the true data distribution because of vanishing variability.

Since GQR takes the training data  $\mathbf{X} \in \mathbb{R}^p$  as input and the target quantile estimate lies in  $\mathbb{R}^1$ , the weights in the DNN associated with  $\mathbf{X} \in \mathbb{R}^p$  are very likely to overwhelm those associated with the noise input  $\tau$ . As a result, GQR is very prone to encountering vanishing variability, as are other generative approaches with multidimensional features. From another point of view, we can see that due to the nonnegativity of the check function, the GQR loss (3) achieves a minimum value of zero when we have vanishing variability (4).

To remedy this problem, we propose a new regularization term that encourages the network to have *more* variability when vanishing variability occurs. Given a set of features  $\mathbf{X} \in \mathbb{R}^p$ , the proposed *variability penalty* is formulated as follows:

$$\text{pen}_{\lambda, \alpha}(G(\mathbf{X}, \tau), G(\mathbf{X}, \tau')) = -\lambda \log \{ \|G(\mathbf{X}, \tau) - G(\mathbf{X}, \tau')\|_1 + 1/\alpha \}, \quad (5)$$

where  $\lambda \geq 0$  is the hyperparameter controlling the degree of penalization,  $\alpha > 0$  is a fixed hyperparameter, and  $\tau, \tau' \sim \text{Uniform}(0, 1)$ . The addition of  $1/\alpha$  inside the logarithmic term of (5) is mainly to ensure that the penalty function is always well-defined (i.e. the quantity inside of  $\log\{\cdot\}$  of (5) cannot equal zero). Our sensitivity analysis in Section C of the Appendix shows that our method is not usually sensitive to the choice of  $\alpha$ . We find that fixing  $\alpha = 1$  or  $\alpha = 5$  works well in practice.

With the addition of the variability penalty (5) to our GQR loss function (3), our *penalized*



GQR (PGQR) method solves the optimization,

$$\widehat{G} = \operatorname{argmin}_{G \in \mathcal{G}^m} \frac{1}{n} \sum_{i=1}^n [\mathbb{E}_{\tau} \{ \rho_{\tau}(Y_i - G(\mathbf{X}_i, \tau)) \} + \mathbb{E}_{\tau, \tau'} \{ \operatorname{pen}_{\lambda, \alpha}(G(\mathbf{X}_i, \tau), G(\mathbf{X}_i, \tau')) \} ], \quad (6)$$

where  $\mathcal{G}^m$  denotes the PMNN family introduced in Section 4, and  $\tau$  and  $\tau'$  independently follow a uniform distribution on  $(0, 1)$ . The expectation  $\mathbb{E}_{\tau, \tau'}$  is again approximated by a Monte Carlo average. Note that when  $\lambda = 0$ , the PGQR loss (6) reduces to the (non-penalized) GQR loss (3).

The next proposition states that an estimated generator function  $\widehat{G}(\mathbf{X}, \tau)$  under the PGQR objective (6) is equivalent to a neural network estimator  $\widehat{g}_{\tau}(\mathbf{X})$  based on the individual (non-integrative) quantile loss function, provided that the family  $\mathcal{G}^m$  in (6) is large enough.

**Proposition 3.1** (equivalence of  $\widehat{g}_{\tau}(\mathbf{X})$  and  $\widehat{G}(\mathbf{X}, \tau)$ ). *For fixed  $\lambda \geq 0$  and  $\alpha > 0$ , let  $\widehat{g}_{\tau}(\mathbf{X}) = \operatorname{argmin}_{g \in \mathcal{H}} \sum_{i=1}^n [\rho_{\tau}(Y_i - g(\mathbf{X}_i)) + \mathbb{E}_{\tau, \tau'} \{ \operatorname{pen}_{\lambda, \alpha}(g(\mathbf{X}_i, \tau), g(\mathbf{X}_i, \tau')) \} ]$ , for a class of neural networks  $\mathcal{H}$ , and  $\tau, \tau' \stackrel{iid}{\sim} \operatorname{Uniform}(0, 1)$ . Consider a class of generator functions  $\mathcal{G}$ , where  $\{G \in \mathcal{G} : \mathbb{R}^p \times \mathbb{R} \times \mathbb{R} \mapsto \mathbb{R}\}$ . Assume that for all  $\mathbf{X} \in \mathcal{X} \subset \mathbb{R}^p$  and quantile levels  $\tau \in (0, 1)$ , there exists  $G \in \mathcal{G}$  such that the target neural network  $\widehat{g}_{\tau}(\mathbf{X})$  can be represented by a hyper-network  $G(\mathbf{X}, \tau)$ . Then, for  $i = 1, \dots, n$ ,*

$$\widehat{g}_{\tau}(\mathbf{X}_i) = \widehat{G}(\mathbf{X}_i, \tau) \quad a.s.,$$

with respect to the probability law related to  $\mathbb{E}_{\tau}$ , where  $\widehat{G}$  is a solution to (6).

*Proof.* See Appendix A. □

Proposition 3.1 justifies optimizing the *integrative* quantile loss over  $\tau$  in the PGQR objective (6). The next proposition justifies adding the variability penalty (5) to the GQR loss (3) by showing that there exists  $\lambda > 0$  so that memorization of the training data does *not* occur under PGQR.

**Proposition 3.2** (PGQR does not memorize the training data). *Suppose that  $\alpha > 0$  is fixed in the variability penalty (5). Denote any minimizer of the PGQR objective function (6) by  $\widehat{G}$ . Then, there exists  $\lambda > 0$  such that*

$$\widehat{G}(\mathbf{X}_i, \tau) \neq Y_i \quad \text{for at least one } i = 1, \dots, n.$$

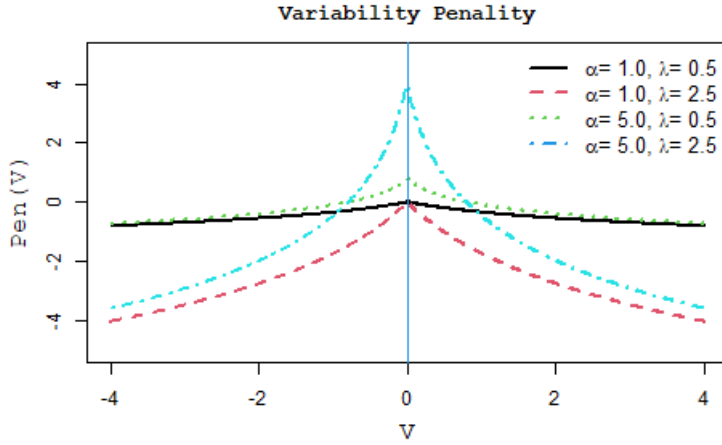


Figure 2: A plot of the penalty function  $\text{pen}_{\lambda,\alpha}(V) = -\lambda \log(|V| + 1/\alpha)$ .

*Proof.* See Appendix A. □

We now provide some intuition into the variability penalty (5). We can quantify the amount of variability in the network by  $V := G(\mathbf{X}, \tau) - G(\mathbf{X}, \tau')$ . Clearly,  $V = 0$  when vanishing variability (4) occurs. To avoid data memorization, we should thus penalize  $V$  *more heavily* when  $V \approx 0$ , with the maximum amount of penalization being applied when  $V = 0$ . Figure 2 plots the variability penalty,  $\text{pen}_{\lambda,\alpha}(V) = -\lambda \log(|V| + 1/\alpha)$ , for several pairs of  $(\alpha, \lambda)$ . Figure 2 shows that  $\text{pen}_{\lambda,\alpha}(V)$  is sharply peaked at zero and that  $\text{pen}_{\lambda,\alpha}(V)$  is strictly convex decreasing in  $|V|$ . Therefore, maximum penalization occurs when each  $V = 0$ , and there is less penalization for larger  $|V|$ . As  $\lambda$  increases,  $\text{pen}_{\lambda,\alpha}(V)$  also increases for all values of  $V \in (-\infty, \infty)$ , indicating that larger values of  $\lambda$  lead to more penalization.

Our penalty function takes a specific form (5). However, any other penalty on  $G(\mathbf{X}, \tau) - G(\mathbf{X}, \tau')$  for  $\mathbf{X} \in \mathcal{X}$  that has a similar shape as the PGQR penalty (i.e. sharply peaked around zero, as in Figure 2) would also conceivably encourage the network to have greater variability. Another way to control the variability is to directly penalize the empirical variance  $s^2 = (n - 1)^{-1} \sum_{i=1}^n [G(\mathbf{X}_i, \tau) - \bar{G}]^2$ , where  $\bar{G} = n^{-1} \sum_{i=1}^n G(\mathbf{X}_i, \tau)$ , or the empirical standard deviation  $s = \sqrt{s^2}$ . However, penalties on  $s^2$  or  $s$  do *not* have an additive form and individual penalty terms depend on each other, and therefore, these are *not* conducive to SGD-based optimization.

We now pause to highlight the novelty of our constructed variability penalty. In many other nonparametric models, e.g. those based on nonparametric smoothing, a roughness penalty is often

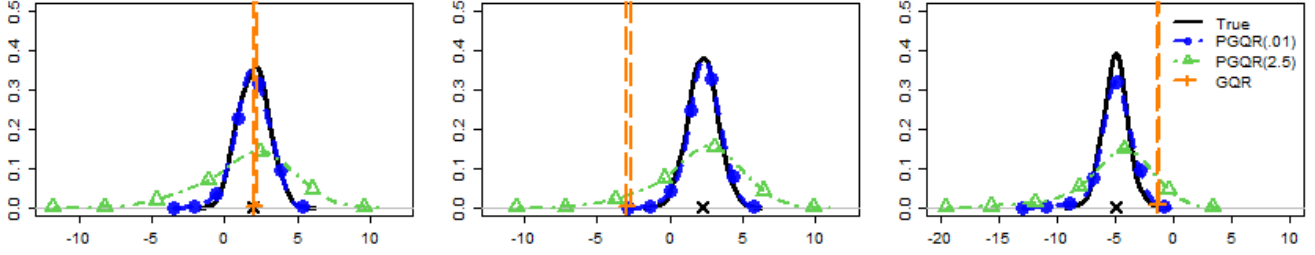


Figure 3: Plots of the estimated conditional densities of  $p(Y | \mathbf{X}_{\text{test}})$  for three different test observations under non-penalized GQR and PGQR with two different choices of  $\lambda \in \{0.01, 2.5\}$ .  $\lambda^* = 0.01$  is the optimal  $\lambda$  chosen by our tuning parameter selection method in Section 5.2.

added to an empirical loss function in order to control the smoothness of the function or density estimate (Green and Silverman, 1994). These roughness penalties encourage greater smoothness of the target function in the spirit of reducing variance in the bias-variance trade-off. In contrast, our variability penalty (5) directly penalizes generators with *too small* variance. By adding the penalty to the GQR loss (3), we are encouraging the estimated network to have *more* variability.

To illustrate how PGQR prevents vanishing variability, we carry out a small simulation study under the model,  $Y_i = \mathbf{X}_i^\top \boldsymbol{\beta} + \epsilon_i, i = 1, \dots, n$ , where  $\mathbf{X}_i \stackrel{iid}{\sim} \mathcal{N}(\mathbf{0}, \mathbf{I}_{20})$ ,  $\epsilon_i \stackrel{iid}{\sim} \mathcal{N}(0, 1)$ , and the coefficients in  $\boldsymbol{\beta}$  are equispaced over  $[-2, 2]$ . We used 2000 samples to train GQR (3) and PGQR (6), and an additional 200 validation samples were used for tuning parameter selection of  $\lambda$  (described in Section 5.2). To train the generative network, we fixed  $\alpha = 1$  and tuned  $\lambda$  from a set of 100 equispaced values between 0 and 2.5. We then generated 1000 samples  $\{\widehat{G}(\mathbf{X}_{\text{test}}, \xi_k, \lambda)\}_{k=1}^{1000}$ ,  $\xi_k \stackrel{iid}{\sim} \text{Uniform}(0, 1)$ , from the estimated conditional density of  $p(Y | \mathbf{X}_{\text{test}})$  for three different choices of out-of-sample test data for  $\mathbf{X}_{\text{test}}$ . In our simulation, the tuning parameter selection procedure introduced in Section 5.2 chose an optimal  $\lambda$  of  $\lambda^* = 0.01$ .

As shown in Figure 3, the *non*-penalized GQR model introduced in Section 3.1 (dashed orange line) suffers from vanishing variability. Namely, GQR generates values near the true test sample  $Y_{\text{test}}$  almost surely, despite the fact that we used 1000 different inputs for  $\xi$  to generate the  $\widehat{G}$  samples. In contrast, the PGQR model with optimal  $\lambda^* = 0.01$  (solid blue line with filled circles) approximates the true conditional density (solid black line) very closely, capturing the Gaussian shape and matching the true underlying variance.

On the other hand, Figure 3 also illustrates that if  $\lambda$  is chosen to be *too large* in PGQR (6),

then the subsequent approximated conditional density will exhibit larger variance than it should. In particular, when  $\lambda = 2.5$ , Figure 3 shows that PGQR (dashed green line with hollow triangles) *overestimates* the true conditional variance for  $Y$  given  $\mathbf{X}$ . This demonstrates that the choice of  $\lambda$  in the variability penalty (2) plays a very crucial role in the practical performance of PGQR. In Section 5.2, we describe how to select an “optimal”  $\lambda$  so that PGQR neither underestimates *nor* overestimates the true conditional variance. Our method for tuning  $\lambda$  also requires only a *single* optimization, making it an attractive and scalable alternative to cross-validation.

## 4 Partial Monotonic Neural Network

Without any constraints on the network, PGQR is just as prone as other unconstrained nonparametric quantile regression models to suffer from crossing quantiles. For a fixed data point  $\mathbf{X}_i$  and an estimated network  $\widehat{G}$ , the *crossing problem* occurs when

$$\widehat{G}(\mathbf{X}_i, \tau_1) > \widehat{G}(\mathbf{X}_i, \tau_2) \text{ when } 0 < \tau_1 < \tau_2 < 1. \quad (7)$$

In the neural network literature, one popular way to address the crossing problem is to add a penalty term to the loss such as  $\max(0, -\partial G(\mathbf{X}_i; \tau)/\partial \tau)$  (Tagasovska and Lopez-Paz, 2018; Liu et al., 2020). Through regularization, the network is encouraged to have larger partial derivatives with respect to  $\tau$ . However, adding this penalty merely alleviates the crossing problem. There is no guarantee that the final model is free of crossing quantiles (Tagasovska and Lopez-Paz, 2018), *or* we may have to keep training the model until the final network is certified to be monotonic with respect to  $\tau$  at the expense of heavy computational cost (Liu et al., 2020). Another natural way to construct a monotonic neural network (MNN) is by restricting the weights of network to be nonnegative through a transformation or through weight clipping (Zhang and Zhang, 1999; Daniels and Velikova, 2010; Mikulincer and Reichman, 2022). Because *all* the weights are constrained to be nonnegative, this class of MNNs might require longer optimization (i.e. more epochs in SGD) and/or a large amount of hidden neurons to ensure the network’s final expressiveness.

Instead of constraining *all* the weights in the neural network, we make a simple modification to the MNN architecture which we call the *partial* monotonic neural network (PMNN). The PMNN

family consists of *two* feedforward neural networks (FNN) as sub-networks which divide the input into two segments. The first sub-network is a weight-constrained quantile network  $\mathbb{R}^1 \mapsto \mathbb{R}^h$  where the only input is the quantile level  $\tau$  and  $h$  denotes the number of hidden neurons. The FNN structure for one hidden layer in this sub-network is  $g(\tau) = \sigma(\mathbf{U}_{\text{pos}}\tau + \mathbf{b})$ , where  $\mathbf{U}_{\text{pos}}$  is the weights matrix of *nonnegative* weights,  $\mathbf{b}$  is the bias matrix, and  $\sigma$  is the activation function, such as the hyperbolic tangent (tanh) function  $\sigma(x) = \tanh(x)$  or the rectified linear unit (ReLU) function  $\sigma(x) = \max\{0, x\}$ . The  $K_1$ -layer constrained sub-network  $g_c$  can then be constructed as  $g_c(\tau) = g_K \circ \dots \circ g_1$ .

The second sub-network is a  $K_2$ -layer *unconstrained* network  $g_{uc} : \mathbb{R}^p \mapsto \mathbb{R}^h$ , taking the data  $\mathbf{X}$  as inputs. The structure of one hidden layer in this sub-network is  $g'(\mathbf{X}) = \sigma(\mathbf{U}\mathbf{X} + \mathbf{b})$ , where  $\mathbf{U}$  is an *unconstrained* weights matrix. We construct  $g_{uc}$  as  $g_{uc}(\mathbf{X}) = g'_{K_2} \circ \dots \circ g'_1$ . Finally, we construct a single weight-constrained connection layer  $f : \mathbb{R}^h \mapsto \mathbb{R}^1$  that connects the two sub-networks to quantile estimators,

$$G(\mathbf{X}, \tau) = f \circ (g_c + g_{uc}). \quad (8)$$

With our PMNN architecture, the monotonicity of  $G(\cdot, \tau)$  with respect to  $\tau$  is guaranteed by the positive weights in the quantile sub-network  $g_c$  and the final layer  $f$ . At the same time, since the data sub-network  $g_{uc}$  is unconstrained in its weights,  $g_{uc}$  can learn the features of the training data well. In particular, the PMNN family is more flexible in its ability to learn features of the data and is easier to optimize than MNN because of this unconstrained sub-network. We use our proposed PMNN architecture as the family  $\mathcal{G}^m$  over which to optimize the PGQR objective for all of the simulation studies and real data analyses in this manuscript.

To investigate the performance of our proposed PMNN family of neural networks, we fit the PGQR model with PMNN as the function class  $\mathcal{G}^m$  on two benchmark datasets. The first dataset is the motorcycles data (Silverman, 1985) where the response variable is head acceleration (in g) and the predictor is time from crash impact (in ms). The second application is a bone mineral density (BMD) dataset (Takeuchi et al., 2006) where the response is the standardized relative change in spinal BMD in adolescents and the predictor is the standardized age of the adolescents. For these two datasets, we estimated the quantile functions at different quantile levels  $\tau \in \{0.1, 0.2, 0.3, 0.4, 0.5, 0.6, 0.7, 0.8, 0.9\}$  over the domain of the predictor. We compared PGQR

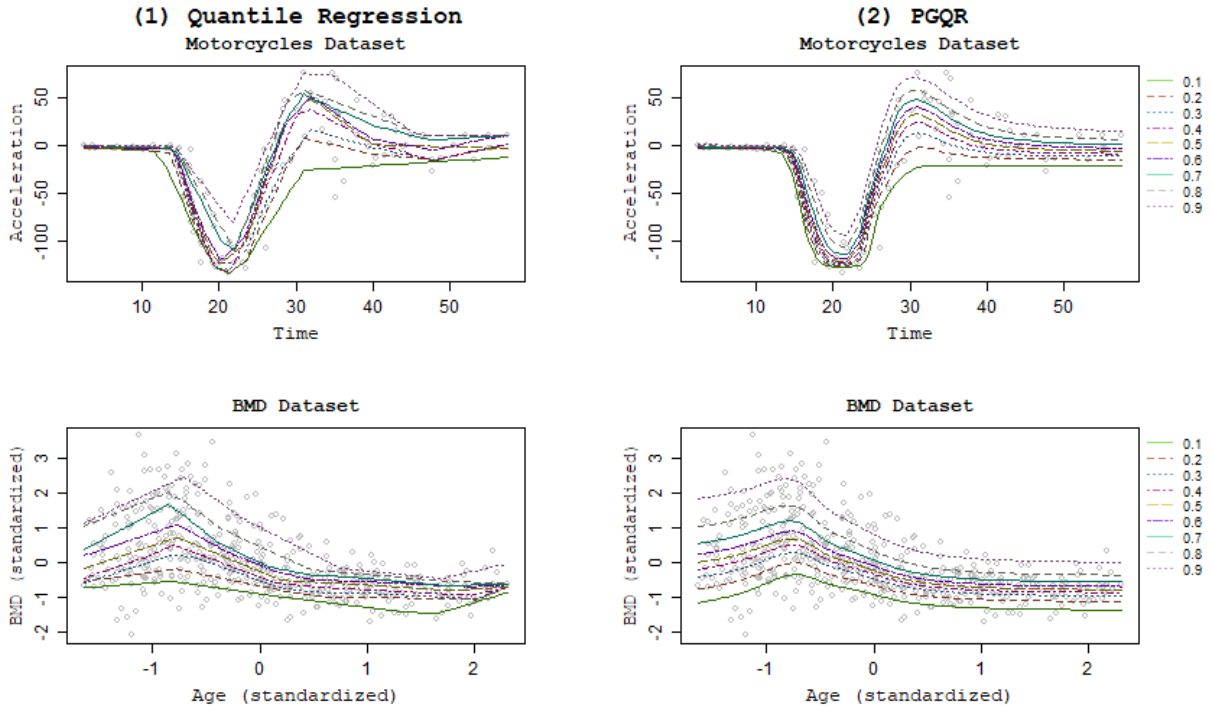


Figure 4: Estimated quantile curves at levels  $\tau \in \{0.1, 0.2, 0.3, 0.4, 0.5, 0.6, 0.7, 0.8, 0.9\}$  for the motorcycle and BMD datasets. The left two panels plot the estimated curves for unconstrained nonparametric quantile regression, and the right two panels plot the estimated curves for PGQR with the PMNN family.

under PMNN to the unconstrained nonparametric quantile regression approach implemented in the R package `quantreg`. The left two panels of Figure 4 demonstrate that the estimated quantile curves under *unconstrained* nonparametric quantile regression are quite problematic for both the motorcycle and BMD datasets; the quantile curves cross each other at multiple points in the predictor domain. In comparison, the right two panels of Figure 4 show that PGQR with the PMNN family ensures *no* crossing quantiles for either dataset.

## 5 Scalable Computation for PGQR

### 5.1 Single-Model Training for PGQR

As illustrated in Section 3.2, PGQR’s performance depends greatly on the regularization parameter  $\lambda \geq 0$  in the variability penalty (5). If  $\lambda$  is too small or if  $\lambda = 0$ , then we may underestimate the true conditional variance of  $p(Y | \mathbf{X})$  and/or encounter the vanishing variability phenomenon. On the other hand, if  $\lambda$  is too large, then we may overestimate the conditional variance.

Due to the large number of parameters in a DNN, tuning  $\lambda$  would be quite burdensome if we had to repeatedly evaluate the deep generative network  $G(\cdot, \tau)$  for multiple choices of  $\lambda$  and training sets. In particular, using cross-validation to tune  $\lambda$  is computationally infeasible for DNNs, especially if the size of the training set is large.

Inspired by the idea of *Generative Multiple-purpose Sampler* (GMS) introduced by Shin et al. (2022), we instead propose to *include*  $\lambda$  as an additional input in the generator, along with data  $\mathbf{X}$  and quantile  $\tau$ . In other words, we impose a discrete uniform distribution  $p(\lambda)$  for  $\lambda$  whose support  $\Lambda$  is a grid of candidate values for  $\lambda$ . We then estimate the network  $G(\cdot, \tau, \lambda)$  with the modified PGQR loss function,

$$\hat{G} = \operatorname{argmin}_{G \in \mathcal{G}^m} \frac{1}{n} \sum_{i=1}^n \mathbb{E}_{\tau, \lambda} \left[ \rho_{\tau}(Y_i - G(\mathbf{X}_i, \tau, \lambda)) + \mathbb{E}_{\tau, \tau'} \{ \operatorname{pen}_{\lambda, \alpha}(G(\mathbf{X}_i, \tau, \lambda), G(\mathbf{X}_i, \tau', \lambda)) \} \right]. \quad (9)$$

Note that (9) differs from the earlier formulation (6) in that  $\lambda \in \Lambda$  is *not* fixed *a priori*. In the PMNN family  $\mathcal{G}^m$ ,  $\lambda$  is included in the unconstrained sub-network  $g_{uc} : \mathbb{R}^{p+1} \mapsto \mathbb{R}^h$ .

The next corollary to Proposition 3.1 justifies including  $\lambda$  in the generator and optimizing the integrative loss over  $\{\tau, \lambda\}$  in the modified PGQR objective (9). The proof of Corollary 5.1 is a straightforward extension of the proof of Proposition 3.1 and is therefore omitted.

**Corollary 5.1.** *Let  $\hat{g}_{\tau, \lambda}(\mathbf{X}) = \operatorname{argmin}_{g \in \mathcal{H}} \sum_{i=1}^n [\rho_{\tau}(Y_i - g(\mathbf{X}_i)) + \mathbb{E}_{\tau, \tau'} \{ \operatorname{pen}_{\lambda, \alpha}(g(\mathbf{X}_i, \tau), g(\mathbf{X}_i, \tau')) \}]$ , for a class of neural networks  $\mathcal{H}$ , where  $\alpha > 0$  is fixed and  $\tau, \tau' \stackrel{iid}{\sim} \operatorname{Uniform}(0, 1)$ . Consider a class of generator functions  $\mathcal{G}$  where  $\{G \in \mathcal{G} : \mathbb{R}^p \times \mathbb{R} \times \mathbb{R} \mapsto \mathbb{R}\}$ . Suppose that for all  $\mathbf{X} \in \mathcal{X} \subset \mathbb{R}^p$ , quantile levels  $\tau \in (0, 1)$ , and tuning parameters  $\lambda \in \Lambda$ , there exists  $G \in \mathcal{G}$  such that the target neural networks  $\hat{g}_{\tau, \lambda}(\mathbf{X})$  can be represented by some  $G(\mathbf{X}, \tau, \lambda)$ . Then, for  $i = 1, \dots, n$ ,*

$$\hat{g}_{\tau, \lambda}(\mathbf{X}_i) = \hat{G}(\mathbf{X}_i, \tau, \lambda) \text{ a.s.,}$$

*with respect to the probability law related to  $\mathbb{E}_{\tau, \lambda}$ , where  $\hat{G}$  is a solution to (9).*

We note that Shin et al. (2022) proposed to use GMS for inference in *linear* quantile regression. In contrast, PGQR is a method for *nonparametric* joint quantile estimation and conditional density estimation (CDE). Linear quantile regression cannot be used for CDE; as a linear model, GMS linear quantile regression also does not suffer from vanishing variability. This is not the case for

GQR, which motivates us to introduce the variability penalty in Section 3.2. Finally, we employ the GMS idea for *tuning parameter* selection in PGQR, rather than for constructing pointwise confidence bands (as in Shin et al. (2022)).

By including  $\lambda \sim p(\lambda)$  in the generator, PGQR only needs to perform one *single* optimization in order to estimate the network  $G$ . We can then *use* the estimated network  $\widehat{G}$  to tune  $\lambda$ , as we detail in the next section. This single-model training stands in contrast to traditional smoothing methods for nonparametric quantile regression, which typically require *repeated* model evaluations via (generalized) cross-validation to tune hyperparameters such as bandwidth or roughness penalty.

## 5.2 Selecting An Optimal Regularization Parameter

We now introduce our method for selecting the regularization parameter  $\lambda$  in our variability penalty (5). Considering the candidate set  $\Lambda$ , the basic idea is to select the best  $\lambda^* \in \Lambda$  that minimizes the distance between the generated conditional distribution and the true conditional distribution.

Denote the trained network under the modified PGQR objective (9) as  $\widehat{G}(\cdot, \tau, \lambda)$ , and let  $(\mathbf{X}_{\text{val}}, Y_{\text{val}})$  denote a validation sample. After optimizing (9), it is effortless to generate the conditional quantile functions for each  $\mathbf{X}_{\text{val}}$  in the validation set, each  $\lambda \in \Lambda$ , and any quantile level  $\xi \in (0, 1)$ . In order to select the optimal  $\lambda^* \in \Lambda$ , we first prove the following proposition.

**Proposition 5.2.** *Suppose that two univariate random variables  $Q$  and  $W$  are independent. Then,  $Q$  and  $W$  have the same distribution if and only if  $P(Q < W \mid W)$  follows a standard uniform distribution.*

*Proof.* See Appendix A. □

Based on Proposition 5.2, we know that, given a validation sample  $(\mathbf{X}_{\text{val}}, Y_{\text{val}})$ , the best  $\lambda^* \in \Lambda$  should satisfy  $P_{\tau, \lambda}(\widehat{G}(\mathbf{X}_{\text{val}}, \tau, \lambda^*) < Y_{\text{val}} \mid Y_{\text{val}}) \sim \text{Uniform}(0, 1)$ . In practice, if we have  $M$  random quantile levels  $\boldsymbol{\tau} = (\tau_1, \dots, \tau_M) \in (0, 1)^M$ , we can estimate the probability  $P_{\tau, \lambda} := P_{\tau, \lambda}(\widehat{G}(\mathbf{X}_{\text{val}}, \tau, \lambda^*) < Y_{\text{val}} \mid Y_{\text{val}})$  with a Monte Carlo approximation,

$$\widehat{P}_{\tau, \lambda}^{(i)} = M^{-1} \sum_{k=1}^M \mathbb{I}\{\widehat{G}(\mathbf{X}_{\text{val}}^{(i)}, \tau_k, \lambda) < Y_{\text{val}}^{(i)}\} \approx P_{\tau, \lambda}(\widehat{G}(\mathbf{X}_{\text{val}}, \tau, \lambda^*) < Y_{\text{val}} \mid Y_{\text{val}}), \quad (10)$$



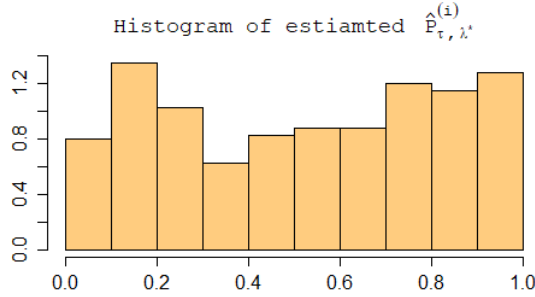


Figure 5: Histogram of the estimated  $\widehat{P}_{\tau, \lambda^*}^{(i)}$ 's in the validation set for the optimal  $\lambda^*$ .

for each  $i$ th validation sample  $(\mathbf{X}_{\text{val}}^{(i)}, Y_{\text{val}}^{(i)})$ . With  $n_{\text{val}}$  validation samples, we proceed to estimate  $\widehat{P}_{\tau, \lambda}^{(i)}$  for all  $n_{\text{val}}$  validation samples  $(\mathbf{X}_{\text{val}}^{(i)}, Y_{\text{val}}^{(i)})$ 's and each  $\lambda \in \Lambda$ . We then compare the empirical distribution of the  $\widehat{P}_{\tau, \lambda}^{(i)}$ 's to a standard uniform distribution for each  $\lambda \in \Lambda$  and select the  $\lambda^*$  that *minimizes* the distance between  $\widehat{P}_{\tau, \lambda}$  and  $\text{Uniform}(0, 1)$ . That is, given a valid distance measure  $d$ , we select the  $\lambda^*$  which satisfies

$$\lambda^* = \underset{\lambda \in \Lambda}{\operatorname{argmin}} d(\widehat{P}_{\tau, \lambda}, \text{Uniform}(0, 1)). \quad (11)$$

There are many possible choices for  $d$  in (11). In this paper, we use the Cramer–von Mises (CvM) criterion due to the simplicity of its computation and its good empirical performance. The CvM criterion is straightforward to compute as

$$d(\widehat{P}_{\tau, \lambda}, \text{Uniform}(0, 1)) = \sum_{i=1}^{n_{\text{val}}} (i/n_{\text{val}} - \widehat{P}_{\tau, \lambda}^{(i)} - 2/n_{\text{val}})^2 / n_{\text{val}}. \quad (12)$$

After selecting  $\lambda^*$  according to (11), we can easily generate samples from the conditional quantiles of  $p(Y | \mathbf{X})$  for any feature data vector  $\mathbf{X}$ . We simply generate  $\widehat{G}(\mathbf{X}, \xi_k, \lambda^*)$ , where  $k = 1, \dots, b$ , for random quantiles  $\xi_1, \dots, \xi_b \stackrel{iid}{\sim} \text{Uniform}(0, 1)$ . For sufficiently large  $b$ , the conditional density  $p(Y | \mathbf{X})$  can be inferred from  $\{\widehat{G}(\mathbf{X}, \xi_k, \lambda^*)\}_{k=1}^b$ . The complete algorithm for scalable computation of PGQR is given in Algorithm 1.

We now illustrate our proposed selection method for  $\lambda \in \Lambda$  in the simulated linear regression example from Section 3.2. Figure 5 plots the histogram of the estimated  $\widehat{P}_{\tau, \lambda^*}^{(i)}$ 's in the validation set for the  $\lambda^*$  which minimizes the CvM criterion. We see that the empirical distribution of the

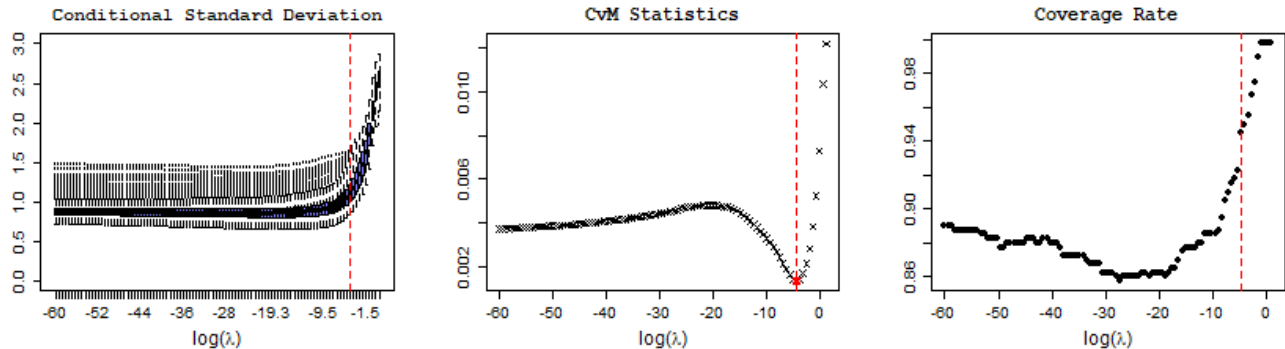


Figure 6: The conditional standard deviation (left panel), CvM statistic (middle panel), and coverage rate (right panel) in the validation set vs.  $\log(\lambda)$  for each  $\lambda \in \Lambda$ . The red dashed line corresponds to the  $\lambda^*$  which minimizes the CvM criterion.

$\widehat{P}_{\tau, \lambda^*}^{(i)}$ 's closely follows a standard uniform distribution.

Figure 6 illustrates how the PGQR solution changes as  $\log(\lambda)$  increases for every  $\lambda \in \Lambda$ . Figure 6 plots the conditional standard deviation (left panel), the CvM criterion (middle panel), and the coverage rate of the 95% confidence intervals (right panel) for the PGQR samples in the validation set. The vertical dashed red line denotes the optimal  $\lambda^* = 0.01$ . We see that the  $\lambda^*$  which minimizes the CvM (middle panel) captures the true conditional standard deviation of  $\sigma = 1$  (left panel) and attains coverage probability close to the nominal rate (right panel). This example demonstrates that our proposed selection method provides a practical alternative to computationally burdensome cross-validation for tuning  $\lambda$  in the variability penalty (5). In Section B.1 of the Appendix, we further demonstrate that our tuning parameter selection method is suitable to use even when the true conditional variance is very small (true  $\sigma^2 = 0.01$ ). In this scenario, our procedure selects a very small  $\lambda^* \approx 0$ , so that PGQR does *not* overestimate the conditional variance.

## 6 Numerical Experiments and Real Data Analysis

We evaluated the performance of PGQR on several simulated and real datasets. We fixed  $\alpha = 1$  or  $\alpha = 5$  in the variability penalty (5). We optimized the modified PGQR loss (9) over the PMNN family (Section 4), where each sub-network had three hidden layers with 1000 neurons per layer. The support for  $\Lambda$  was chosen to be 100 equispaced values between 0 and 1. We compared PGQR to several other state-of-the-art methods:

---

**Algorithm 1** Scalable Implementation of PGQR

---

```
1: Split non-test data into non-overlapping training set ( $\mathbf{X}_{\text{train}}, \mathbf{Y}_{\text{train}}$ ) and validation set ( $\mathbf{X}_{\text{val}}, \mathbf{Y}_{\text{val}}$ )
2: Initialize  $G$  parameters  $\phi$ , learning rate  $\gamma$ , width  $h$  of DNN hidden layers, and total epoches  $T$ 
3: procedure: Optimizing  $G$ 
4:   for epoch  $t$  in  $1, \dots, T$  do
5:     Sample  $\tau, \tau' \sim \text{Uniform}(0, 1)$  and  $\lambda \in \Lambda$ 
6:     Evaluate loss (9) with ( $\mathbf{X}_{\text{train}}, \mathbf{Y}_{\text{train}}$ )
7:     Update  $G$  parameters  $\phi$  via SGD
8:   end for
9:   return  $\hat{G}$ 
10: end procedure
11: procedure: Tuning  $\lambda$ 
12:   Set  $M = 1000$  and sample  $\tau_1, \dots, \tau_M \stackrel{iid}{\sim} \text{Uniform}(0, 1)$ 
13:   Generate  $\{\hat{G}(\mathbf{X}_{\text{val}}^{(i)}, \tau_1, \lambda_l), \dots, \hat{G}(\mathbf{X}_{\text{val}}^{(i)}, \tau_M, \lambda_l)\}$  for each  $\lambda_l \in \Lambda$  and each  $\mathbf{X}_{\text{val}}^{(i)}, i = 1, \dots, n_{\text{val}}$ 
14:   Compute  $\hat{P}_{\tau, \lambda_l}^{(i)}$  as in (10) on ( $\mathbf{X}_{\text{val}}^{(i)}, Y_{\text{val}}^{(i)}$ ) for each  $i = 1, \dots, n_{\text{val}}$  and each  $\lambda_l \in \Lambda$ 
15:   Select  $\lambda^*$  according to (11) with CvM criterion (12) as  $d$ 
16:   return  $\lambda^*$ 
17: end procedure
18: procedure: Estimating  $p(Y | \mathbf{X}_{\text{test}})$  for test data  $\mathbf{X}_{\text{test}}$ 
19:   Set  $b = 1000$  and sample  $\xi_1, \dots, \xi_b \stackrel{iid}{\sim} \text{Uniform}(0, 1)$ 
20:   Estimate  $\xi_k$ -th quantile of  $Y | \mathbf{X}_{\text{test}}$  as  $\hat{G}(\mathbf{X}_{\text{test}}, \xi_k, \lambda^*)$  for  $k = 1, \dots, b$ 
21:   return  $\{\hat{G}(\mathbf{X}_{\text{test}}, \xi_1, \lambda^*), \dots, \hat{G}(\mathbf{X}_{\text{test}}, \xi_b, \lambda^*)\}$ 
22: end procedure
```

---

- **GCDS** (Zhou et al., 2022). Following Zhou et al. (2022), we trained both a generator and a discriminator using FNNs with one hidden layer of 25 neurons. Despite this simple architecture, we found that GCDS might still encounter vanishing variability. For fair comparison to PGQR, we also increased the number of hidden layers to three and the number of nodes per layer to 1000. We refer to this modification as **deep-GCDS**.
- **WGCS** (Liu et al., 2021). We adopted the gradient penalty recommended by Liu et al. (2021) and set the hyperparameter associated with the gradient penalty as 0.1.
- **FlexCoDE** (Izbicki and Lee, 2017). We considered three ways of estimating the basis functions  $\beta_j(\mathbf{X})$ : nearest-neighbor regression (NNR), sparse additive model (SAM), and XGBoost (FlexZboost).
- **Random Forest CDE**, or RFCDE (Pospisil and Lee, 2019).

For FlexCoDE and RFCDE, we adopted the default hyperparameter settings of Izbicki and Lee (2017) and Pospisil and Lee (2019) respectively.

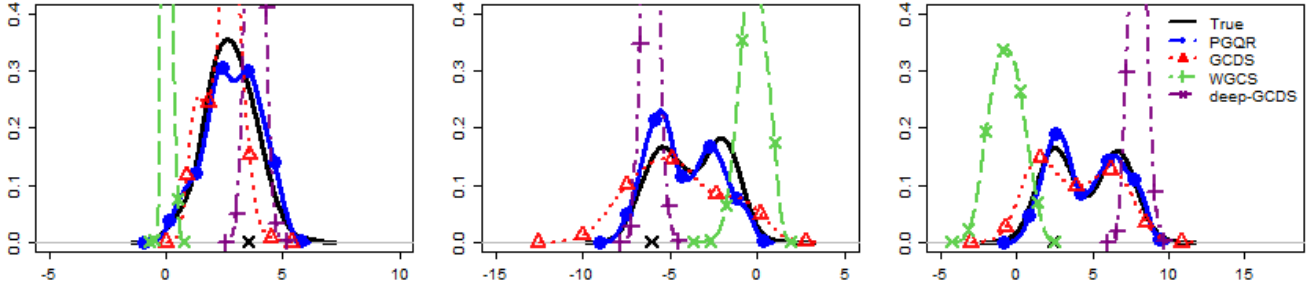


Figure 7: Plots of the estimated conditional densities of  $p(Y | \mathbf{X}_{\text{test}})$  for three different test observations from one replication of Simulation 3. Plotted are the estimated conditional densities for PGQR ( $\alpha = 1$ ), GCDS, WGCS, and deep-GCDS.

## 6.1 Simulation Studies

For our simulation studies, we generated data from  $Y_i = g(\mathbf{X}_i) + \epsilon_i, i = 1, \dots, 2000$ , for some function  $g$ , where  $\mathbf{X}_i \stackrel{iid}{\sim} \mathcal{N}(\mathbf{0}, \mathbf{I}_p)$  and the residual errors  $\epsilon_i$ 's were independent. The specific simulation settings are described below.

1. **Simulation 1: Multimodal and heteroscedastic.**  $Y_i = \beta_i X_i + \epsilon_i$ , where  $\beta_i = \{-1, 0, 1\}$  with equal probability and  $\epsilon_i = (0.25 \cdot |X_i|)^{1/2}$ .
2. **Simulation 2: Mixture of left-skewed and right-skewed.**  $Y_i = \mathbf{X}_i^\top \boldsymbol{\beta} + \epsilon_i$ , where  $\boldsymbol{\beta} \in \mathbb{R}^5$  is equispaced between  $[-2, 2]$ , and  $\epsilon_i = \chi^2(1, 1)\mathcal{I}(X_1 \geq 0.5) + \log[\chi^2(1, 1)]\mathcal{I}(X_1 < 0.5)$ . Here, the skewness is controlled by the covariate  $X_1$ .
3. **Simulation 3: Mixture of unimodal and bimodal.**  $Y_i = \mathbf{X}_i^\top \boldsymbol{\beta}_i + \epsilon_i$ , where  $\boldsymbol{\beta}_i \in \mathbb{R}^5$  with  $\beta_{i1} \in \{-2, 2\}$  with equal probability,  $(\beta_{i2}, \beta_{i3}, \beta_{i4}, \beta_{i5})^\top$  are equispaced between  $[-2, 2]$ , and  $\epsilon_i \stackrel{iid}{\sim} \mathcal{N}(0, 1)$ . Here,  $p(Y | \mathbf{X})$  is unimodal when  $X_1 \approx 0$ , and otherwise, it is bimodal.

In our simulations, 80% of the data was used to train the model, 10% was used as the validation set for tuning parameter selection, and the remaining 10% was used as test data to evaluate model performance. In Section B.1 of the Appendix, we present additional results where  $g(\mathbf{X}_i)$  is a nonlinear function of  $\mathbf{X}_i$  (Simulation 4) and where the error variance is very small (Simulation 5).

Figure 7 compares the estimated conditional density of  $p(Y | \mathbf{X}_{\text{test}})$  for three test observations from one replication of Simulation 3. We see that PGQR (solid blue line with filled circles) is able to capture both the unimodality *and* the bimodality of the ground truth conditional densities (solid black line). Meanwhile, GCDS (dashed red line with hollow triangles), WGCS (dashed

Method	Simulation 1			Simulation 2			Simulation 3		
	$\mathbb{E}(Y   \mathbf{X})$	$\text{sd}(Y   \mathbf{X})$	Cov (Width)	$\mathbb{E}(Y   \mathbf{X})$	$\text{sd}(Y   \mathbf{X})$	Cov (Width)	$\mathbb{E}(Y   \mathbf{X})$	$\text{sd}(Y   \mathbf{X})$	Cov (Width)
PGQR ( $\alpha=1$ )	0.41	0.34	0.95 (23.48)	0.38	0.11	0.93 (8.14)	0.30	0.08	0.92 (6.61)
PGQR ( $\alpha=5$ )	<b>0.36</b>	<b>0.31</b>	0.95 (23.41)	<b>0.31</b>	<b>0.07</b>	<b>0.95 (8.83)</b>	<b>0.25</b>	<b>0.06</b>	<b>0.96 (6.60)</b>
GCDS	10.49	25.82	0.68 (15.48)	0.53	0.27	0.92 (8.55)	0.33	0.12	0.84 (5.78)
WGCS	229.91	73.68	0.15 (4.88)	6.57	1.45	0.80 (9.17)	6.25	1.98	0.71 (8.08)
deep-GCDS	7.99	56.87	0.38 (7.42)	5.41	2.89	0.42 (2.12)	6.11	2.78	0.28 (2.04)
FlexCoDE-NNR	0.97	0.54	0.96 (23.94)	0.83	0.36	0.91 (9.03)	1.12	0.75	0.92 (9.11)
FlexCoDE-SAM	0.37	0.62	0.97 (25.07)	0.73	1.03	0.93 (11.15)	1.01	1.99	0.93 (10.91)
FlexZBoost	0.77	63.81	<b>1.00 (46.11)</b>	1.29	0.36	0.91 (8.28)	1.77	0.74	0.85 (7.88)
RFCDE	1.98	0.72	0.44 (25.46)	0.61	0.34	0.56 (6.26)	0.83	0.65	0.96 (23.06)

Table 1: Table reporting the PMSE for the conditional expectation and standard deviation, as well as the coverage rate (Cov) and average width of the 95% prediction intervals, for Simulations 1 through 3. Results were averaged across 20 replicates.

green line with crosses), and deep-GCDS (dashed purple line with plusses) struggled to capture the true conditional densities for at least some test points. In particular, Figure 7 shows some evidence of variance *underestimation* for WGCS and deep-GCDS, whereas this is counteracted by the variability penalty in PGQR. Additional figures from our simulation studies are provided in Section B.2 of the Appendix.

We repeated our simulations for 20 replications. For each experiment, we computed the predicted mean squared error (PMSE) for different summaries of the conditional densities for the test data. We define the PMSE as

$$\text{PMSE} = \frac{1}{n_{\text{test}}} \sum_{i=1}^{n_{\text{test}}} (\hat{m}(\mathbf{X}_{\text{test},i}) - m(\mathbf{X}_{\text{test},i}))^2, \quad (13)$$

where  $m(\mathbf{X})$  generically refers to the conditional mean of  $Y$  given  $\mathbf{X}$ , i.e.  $\mathbb{E}(Y | \mathbf{X})$ , or the conditional standard deviation, i.e.  $\text{sd}(Y | \mathbf{X})$ . For the generative models (PGQR, GCDS, WGCS, and deep-GCDS), we approximated  $\hat{m}$  in (13) by Monte Carlo simulation using 1000 generated samples, while for FlexCoDE and RFCDE, we approximated  $\hat{m}$  using numerical integration. In addition to PMSE, we also used the 2.5th and 97.5th percentiles of the predicted conditional densities to construct 95% prediction intervals for the test data. We then calculated the coverage probability (Cov) and the average width for these prediction intervals.

Table 1 summarizes the results for PGQR with  $\alpha \in \{1, 5\}$  in (5) and all competing methods, averaged across 20 experiments. There was not much substantial difference between  $\alpha = 1$  and  $\alpha = 5$  for PGQR. Table 1 shows that PGQR had the lowest PMSE in all three simulations

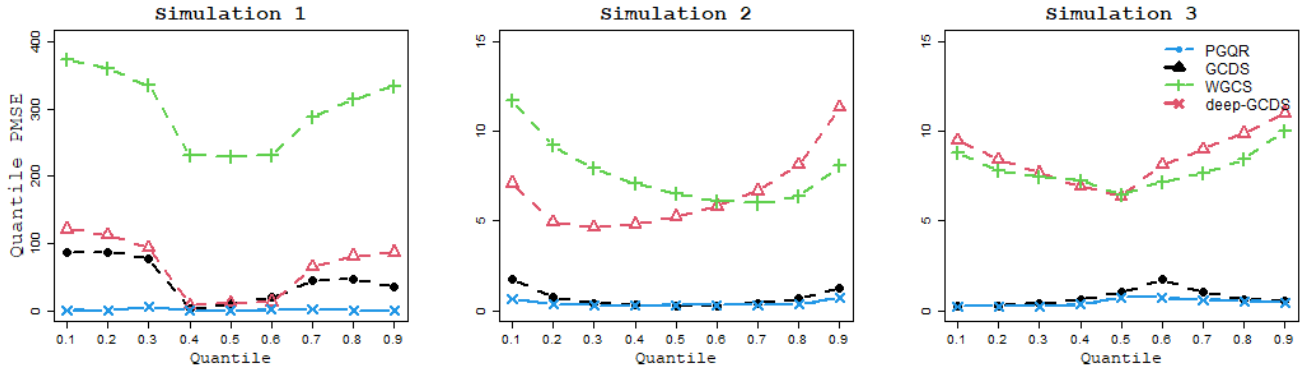


Figure 8: Plot of the average PMSE across 20 replicates for the  $\tau$ -th quantiles  $Q_{Y|\mathbf{X}}(\tau)$ ,  $\tau \in \{0.1, 0.2, 0.3, 0.4, 0.5, 0.6, 0.7, 0.8, 0.9\}$  for Simulations 1 through 3.

and attained coverage close to the nominal rate. In Simulations 2 and 3, the prediction intervals produced by PGQR had the highest coverage rate. In Simulation 1, FlexZBoost had 100% coverage, but the average width of the prediction intervals for FlexZBoost was considerably larger than that of the other methods, suggesting that the intervals produced by FlexZBoost may be too conservative to be informative.

We also computed the PMSE for the  $\tau$ -th quantile. Figure 8 plots the PMSE for these nine quantiles for PGQR ( $\alpha = 1$ ), GCDS, deep-GCDS, and WGCS, averaged across 20 experiments. We see that PGQR (blue line with crosses) had the lowest PMSE for most of the quantile levels. PGQR also had uniformly lower PMSE in our quantile set than WGCS (green line with pluses) and deep-GCDS (red line with triangles), suggesting that WGCS and deep-GCDS may have been more prone to vanishing variability.

## 6.2 Real Data Analysis

We also examined the performance of PGQR on three real datasets from the UCI Machine Learning Repository, which we denote as: `machine`, `fish`, and `noise`.<sup>1</sup> The `machine` dataset comes from a real experiment that collected the excitation current ( $Y$ ) and four machine attributes ( $\mathbf{X}$ ) for a set of synchronous motors (Kahraman, 2014). The `fish` dataset contains the concentration of aquatic toxicity ( $Y$ ) that can cause death in fathead minnows and six molecular descriptors ( $\mathbf{X}$ ) described in (Cassotti et al., 2015). The `noise` dataset measures the scaled sound pressure in decibels ( $Y$ )

<sup>1</sup>Accessed from <https://archive.ics.uci.edu/ml/index.php>.

Dataset	$n$	$p$	PGQR		GCDS		deep-GCDS		WGCS	
			Cov	Width	Cov	Width	Cov	Width	Cov	Width
machine	557	4	<b>0.96</b>	2.82	0.91	1.92	0.87	1.52	0.69	1.66
fish	908	6	<b>0.96</b>	3.29	0.79	2.38	0.54	1.08	0.80	2.36
noise	1503	5	<b>0.92</b>	7.58	0.00	1.68	0.00	0.24	0.00	22.41

Table 2: Results from our real data analysis. Cov and width denote the coverage rate and average width respectively of the 95% prediction intervals for the test observations.

at different frequencies, angles of attacks, wind speed, chord length, and suction side displacement thickness ( $\mathbf{X}$ ) for a set of airfoils (Lopez et al., 2008). Table 2 reports the sample size  $n$  and covariate dimension  $p$  for these three benchmark datasets.

We examined the out-of-sample performance for PGQR (with fixed  $\alpha = 1$ ), GCDS, deep-GCDS, and WGCS. In particular, 80% of each dataset was randomly selected as training data, 10% was used as validation data for tuning parameter selection, and the remaining 10% was used as test data for model evaluation. To compare these deep generative methods, we considered the out-of-sample coverage rate (Cov) and the average width of the 95% prediction intervals in the test data.

The results from our real data analysis are summarized in Table 2. We see that on all three datasets, PGQR achieved higher coverage that was closer to the nominal rate than the competing methods. It seems as though the other generative approaches may have been impacted by the vanishing variability phenomenon, resulting in too narrow prediction intervals that did not cover as many test samples. In particular, GCDS, deep-GCDS, and WGCS all performed extremely poorly on the `noise` dataset, with an out-of-sample coverage rate of zero. On the other hand, with the help of the variability penalty (5), PGQR did *not* underestimate the variance and demonstrated an overwhelming advantage over these other methods in terms of predictive power. Moreover, the average widths of the PGQR prediction intervals were not overwhelmingly large so as to be uninformative.

Figure 9 plots the PGQR 95% prediction intervals for the test observations ordered in ascending order. The red crosses depict test samples that were *not* captured by their corresponding PGQR prediction intervals. We do not detect any specific pattern for the uncaptured test points, indicating reasonable generalizability for the PQGR model.

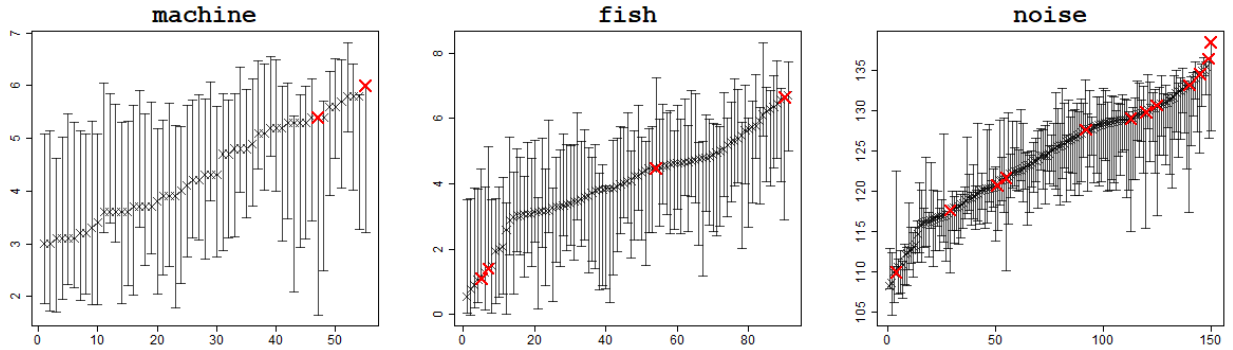


Figure 9: The PGQR 95% prediction intervals for the test samples in the three benchmark datasets. The red crosses indicate the test points that were not captured by their corresponding prediction intervals.

## 7 Discussion

In this paper, we have made contributions to both the quantile regression and deep learning literature. Specifically, we proposed PGQR as a new deep generative approach to joint quantile estimation and conditional density estimation. Different from existing conditional sampling methods (Zhou et al., 2022; Liu et al., 2021), PGQR employs a novel variability penalty to counteract the *vanishing variability* phenomenon in deep generative networks. We introduced the PMNN family of neural networks to enforce the monotonicity of quantile functions. Finally, we provided a scalable implementation of PGQR which requires solving only a single optimization to select the regularization term in the variability penalty. Through analyses of real and simulated datasets, we demonstrated PGQR’s ability to capture critical aspects of the conditional distribution such as multimodality, heteroscedasticity, and skewness.

We anticipate that our penalty on vanishing variability in generative networks is broadly applicable for a wide number of loss functions besides the check function. In the future, we will extend the variability penalty to other deep generative models and other statistical problems besides quantile regression. In addition, we plan to pursue variable selection, so that our method can also identify the most relevant covariates when the number of features  $p$  is large. Owing to its single-model training, PGQR is scalable for large  $n$ . However, further improvements are needed in order for PGQR to avoid the curse of dimensionality for large  $p$ .



# Acknowledgments

The last author was generously supported by NSF grant DMS-2015528. The authors are grateful to Dr. Jun Liu for helpful comments.

# References

- Arora, S., Ge, R., Liang, Y., Ma, T., and Zhang, Y. (2017). Generalization and equilibrium in generative adversarial nets (GANs). In Precup, D. and Teh, Y. W., editors, *Proceedings of the 34th International Conference on Machine Learning*, volume 70 of *Proceedings of Machine Learning Research*, pages 224–232. PMLR.
- Arpit, D., Jastrzundefinedbski, S., Ballas, N., Krueger, D., Bengio, E., Kanwal, M. S., Maharaj, T., Fischer, A., Courville, A., Bengio, Y., and Lacoste-Julien, S. (2017). A closer look at memorization in deep networks. In *Proceedings of the 34th International Conference on Machine Learning - Volume 70, ICML'17*, page 233–242. JMLR.org.
- Cannon, A. J. (2018). Non-crossing nonlinear regression quantiles by monotone composite quantile regression neural network, with application to rainfall extremes. *Stochastic Environmental Research and Risk Assessment*, 32(11):3207–3225.
- Cassotti, M., Ballabio, D., Todeschini, R., and Consonni, V. (2015). A similarity-based QSAR model for predicting acute toxicity towards the fathead minnow (*pimephales promelas*). *SAR and QSAR in Environmental Research*, 26(3):217–243.
- Chaudhuri, P. and Loh, W.-Y. (2002). Nonparametric estimation of conditional quantiles using quantile regression trees. *Bernoulli*, 8(5):561–576.
- Dabney, W., Ostrovski, G., Silver, D., and Munos, R. (2018). Implicit quantile networks for distributional reinforcement learning. In Dy, J. and Krause, A., editors, *Proceedings of the 35th International Conference on Machine Learning*, volume 80 of *Proceedings of Machine Learning Research*, pages 1096–1105. PMLR.
- Daniels, H. and Velikova, M. (2010). Monotone and partially monotone neural networks. *IEEE Transactions on Neural Networks*, 21(6):906–917.
- Emmert-Streib, F., Yang, Z., Feng, H., Tripathi, S., and Dehmer, M. (2020). An introductory review of deep learning for prediction models with big data. *Frontiers in Artificial Intelligence*, 3.
- Evans, W. J. (2010). Skeletal muscle loss: cachexia, sarcopenia, and inactivity. *The American Journal of Clinical Nutrition*, 91(4):1123S–1127S.
- Goodfellow, I., Pouget-Abadie, J., Mirza, M., Xu, B., Warde-Farley, D., Ozair, S., Courville, A., and Bengio, Y. (2014). Generative adversarial nets. In Ghahramani, Z., Welling, M., Cortes, C., Lawrence, N., and Weinberger, K., editors, *Advances in Neural Information Processing Systems*, volume 27. Curran Associates, Inc.
- Green, P. J. and Silverman, B. W. (1994). *Nonparametric Regression and Generalized Linear Models: A Roughness Penalty Approach*. Chapman and Hall.
- Izbicki, R. and Lee, A. B. (2017). Converting high-dimensional regression to high-dimensional conditional density estimation. *Electronic Journal of Statistics*, 11(2):2800–2831.
- Jiang, R., Zhou, Z.-G., Qian, W.-M., and Shao, W.-Q. (2012a). Single-index composite quantile regression. *Journal of the Korean Statistical Society*, 41(3):323–332.
- Jiang, X., Jiang, J., and Song, X. (2012b). Oracle model selection for nonlinear models based on weighted composite quantile regression. *Statistica Sinica*, 22(4):1479–1506.
- Jin, J. and Zhao, Z. (2021). Composite quantile regression neural network for massive datasets. *Mathematical Problems in Engineering*, 2021.

- Kahraman, H. T. (2014). Metaheuristic linear modeling technique for estimating the excitation current of a synchronous motor. *Turkish Journal of Electrical Engineering and Computer Sciences*, 22(6):1637–1652.
- Koenker, R. and Bassett Jr, G. (1982). Robust tests for heteroscedasticity based on regression quantiles. *Econometrica*, 50(1):43–61.
- Koenker, R., Chernozhukov, V., He, X., and Peng, L. (2017). *Handbook of Quantile Regression*. CRC press.
- Koenker, R. and Hallock, K. F. (2001). Quantile regression. *Journal of Economic Perspectives*, 15(4):143–156.
- Koenker, R., Ng, P., and Portnoy, S. (1994). Quantile smoothing splines. *Biometrika*, 81(4):673–680.
- Li, D., Li, Q., and Li, Z. (2021). Nonparametric quantile regression estimation with mixed discrete and continuous data. *Journal of Business & Economic Statistics*, 39(3):741–756.
- Liu, S., Zhou, X., Jiao, Y., and Huang, J. (2021). Wasserstein generative learning of conditional distribution. *arXiv preprint arXiv:2112.10039*.
- Liu, X., Han, X., Zhang, N., and Liu, Q. (2020). Certified monotonic neural networks. In Larochelle, H., Ranzato, M., Hadsell, R., Balcan, M., and Lin, H., editors, *Advances in Neural Information Processing Systems*, volume 33, pages 15427–15438. Curran Associates, Inc.
- Lopez, R., Balsa-Canto, E., and Onate, E. (2008). Neural networks for variational problems in engineering. *International Journal for Numerical Methods in Engineering*, 75(11):1341–1360.
- Lu, Z., Pu, H., Wang, F., Hu, Z., and Wang, L. (2017). The expressive power of neural networks: A view from the width. In Guyon, I., Luxburg, U. V., Bengio, S., Wallach, H., Fergus, R., Vishwanathan, S., and Garnett, R., editors, *Advances in Neural Information Processing Systems*, volume 30. Curran Associates, Inc.
- Meinshausen, N. (2006). Quantile regression forests. *Journal of Machine Learning Research*, 7(35):983–999.
- Mikulincer, D. and Reichman, D. (2022). Size and depth of monotone neural networks: interpolation and approximation. *arXiv preprint arXiv:2207.05275*.
- Moon, S. J., Jeon, J.-J., Lee, J. S. H., and Kim, Y. (2021). Learning multiple quantiles with neural networks. *Journal of Computational and Graphical Statistics*, 30(4):1238–1248.
- Pospisil, T. and Lee, A. B. (2019). RFCDE: Random forests for conditional density estimation and functional data. *arXiv preprint arXiv:1804.05753*.
- RoyChoudhury, A. and Xu, C. (2020). A dataset on body composition, strength and performance in older adults. *Data in Brief*, 29:105103.
- Sangnier, M., Fercoq, O., and d'Alché-Buc, F. (2016). Joint quantile regression in vector-valued RKHSs. In Lee, D., Sugiyama, M., Luxburg, U., Guyon, I., and Garnett, R., editors, *Advances in Neural Information Processing Systems*, volume 29. Curran Associates, Inc.
- Scafoglieri, A., Clarys, J. P., Bauer, J. M., Verlaan, S., Van Malderen, L., Vantieghem, S., Cederholm, T., Sieber, C. C., Mets, T., and Bautmans, I. (2017). Predicting appendicular lean and fat mass with bioelectrical impedance analysis in older adults with physical function decline – the provide study. *Clinical Nutrition*, 36(3):869–875.
- Shin, M., Wang, S., and Liu, J. S. (2022). Generative multiple-purpose sampler for weighted M-estimation. *arXiv preprint arXiv:2006.00767*.
- Silverman, B. W. (1985). Some aspects of the spline smoothing approach to non-parametric regression curve fitting. *Journal of the Royal Statistical Society: Series B (Methodological)*, 47(1):1–21.
- Tagasovska, N. and Lopez-Paz, D. (2018). Frequentist uncertainty estimates for deep learning. *arXiv preprint arXiv:1811.00908*.
- Takeuchi, I., Le, Q., Sears, T., Smola, A., et al. (2006). Nonparametric quantile estimation. *Journal of Machine Learning Research*, 7(45):1231–1264.

- Taylor, J. W. (2000). A quantile regression neural network approach to estimating the conditional density of multiperiod returns. *Journal of Forecasting*, 19(4):299–311.
- van den Burg, G. and Williams, C. (2021). On memorization in probabilistic deep generative models. In Ranzato, M., Beygelzimer, A., Dauphin, Y., Liang, P., and Vaughan, J. W., editors, *Advances in Neural Information Processing Systems*, volume 34, pages 27916–27928. Curran Associates, Inc.
- Xu, Q., Deng, K., Jiang, C., Sun, F., and Huang, X. (2017). Composite quantile regression neural network with applications. *Expert Systems with Applications*, 76:129–139.
- Zhang, H. and Zhang, Z. (1999). Feedforward networks with monotone constraints. In *IJCNN'99. International Joint Conference on Neural Networks. Proceedings (Cat. No.99CH36339)*, volume 3, pages 1820–1823 vol.3.
- Zhou, X., Jiao, Y., Liu, J., and Huang, J. (2022). A deep generative approach to conditional sampling. *Journal of the American Statistical Association (to appear)*.
- Zou, H. and Yuan, M. (2008). Composite quantile regression and the oracle model selection theory. *The Annals of Statistics*, 36(3):1108–1126.

## A Proofs of Propositions

**Proof of Proposition 3.1.** Suppose that for some  $\epsilon > 0$ , there exists a set  $\mathcal{C} \subset (0, 1)$  with  $P_\tau(\mathcal{C}) > \epsilon$  such that for some  $i^* \in \{1, \dots, n\}$ ,  $\hat{g}_\tau(\mathbf{X}_{i^*}) \neq \hat{G}(\mathbf{X}_{i^*}, \tau)$  for all  $\tau \in \mathcal{C}$ . Then we can construct another optimal generator  $\tilde{G}$  such that

$$\begin{aligned} & \frac{1}{n} \sum_{i=1}^n \mathbb{E}_\tau \left[ \rho_\tau(y_i - \hat{G}(\mathbf{X}_i, \tau)) \right] + \mathbb{E}_{\tilde{\tau}, \tilde{\tau}'} \left\{ \text{pen}_{\lambda, \alpha} \left( \hat{G}(\mathbf{X}_i, \tilde{\tau}), \hat{G}(\mathbf{X}_i, \tilde{\tau}') \right) \right\} \\ & \geq \frac{1}{n} \sum_{i=1}^n \mathbb{E}_\tau \left[ \rho_\tau(y_i - \tilde{G}(\mathbf{X}_i, \tau)) \right] + \mathbb{E}_{\tilde{\tau}, \tilde{\tau}'} \left\{ \text{pen}_{\lambda, \alpha} \left( \tilde{G}(\mathbf{X}_i, \tilde{\tau}), \tilde{G}(\mathbf{X}_i, \tilde{\tau}') \right) \right\}, \end{aligned}$$

where

$$\tilde{G}(\mathbf{X}_{i^*}, \tau) = \begin{cases} \hat{G}(\mathbf{X}_{i^*}, \tau) & \text{for } \tau \notin \mathcal{C}, \\ \hat{g}_\tau(\mathbf{X}_{i^*}) & \text{for } \tau \in \mathcal{C}. \end{cases}$$

This is a contradiction due to the fact that  $\hat{g}_\tau$  is the minimizer of  $\frac{1}{n} \sum_{i=1}^n \rho_\tau(y_i - \hat{G}(\mathbf{X}_i, \tau)) + \mathbb{E}_{\tilde{\tau}, \tilde{\tau}'} \{ \text{pen}_{\lambda, \alpha}(\hat{G}(\mathbf{X}_i, \tilde{\tau}), \hat{G}(\mathbf{X}_i, \tilde{\tau}')) \}$ .  $\square$

**Proof of Proposition 3.2.** Suppose that for all  $\lambda \geq 0$ , all  $\tau \in (0, 1)$ , and all  $i \in \{1, \dots, n\}$ ,

$$\hat{G}(\mathbf{X}_i, \tau) = Y_i.$$

Then the penalty part in the PGQR loss (6) attains  $\mathbb{E}_{\tau, \tau'} \{\text{pen}_{\lambda, \alpha}(\widehat{G}(\mathbf{X}_i, \tau), \widehat{G}(\mathbf{X}_i, \tau'))\} = \lambda \log(\alpha)$ , while the first term in (6) satisfies  $\mathbb{E}_{\tau} [\rho_{\tau}(y_i - \widehat{G}(\mathbf{X}_i, \tau))] = 0$ . As a result, the total loss is  $\lambda \log(\alpha)$ .

Since the case of  $\widehat{G}(\mathbf{X}_i, \tau) = Y_i$  is included in cases of  $\text{Var}_{\tau} \{\widehat{G}(\mathbf{X}_i, \tau)\} = 0$ , we focus on the variance. When there exists some  $i \in \{1, \dots, n\}$  and some  $\tau \in (0, 1)$  such that

$$\text{Var}_{\tau} \left\{ \widehat{G}(\mathbf{X}_i, \tau) \right\} > 0,$$

the resulting total loss can be made less than  $\lambda \log(\alpha)$  by choosing an appropriate  $\lambda > 0$ . This contradicts the fact that  $\widehat{G}$  is the minimizer as in (6).  $\square$

**Proof of Proposition 5.2.** It is trivial that  $F_Q(W) := P(Q \leq W \mid W) \sim \text{Uniform}(0, 1)$  when  $Q \stackrel{d}{=} W$ . WLOG, we assume that  $F_Q$  is invertible. We shall show that  $F_Q(W) \sim \text{Uniform}(0, 1)$  implies that the two distributions for  $Q$  and  $W$  are identical. Suppose that  $F_Q(W)$  follows a standard uniform distribution. Then,

$$x = P(F_Q(W) < x) = P(W < F_Q^{-1}(x)) = F_Q(F_Q^{-1}(x)),$$

which implies that  $F_W(F_W^{-1}(x)) = x$ . Thus, it follows that the distributions of  $Q$  and  $W$  are identical.  $\square$

## B More Simulation Results

### B.1 Additional Simulation Studies

In addition to the three simulations described in Section 6 of the main manuscript, we also conducted simulation studies under the following scenarios:

- **Simulation 4: Nonlinear function with an interaction term and one irrelevant covariate.**  $Y_i = 0.5 \log(10 - X_{i1}^2) + 0.75 \exp(X_{i2}X_3/5) - 0.25|X_{i4}/2| + \epsilon_i$ , where  $\epsilon_i \sim \mathcal{N}(0, 1)$ . Note that there is a (nonlinear) interaction between  $X_2$  and  $X_3$ , while  $X_5$  is irrelevant.
- **Simulation 5: Very small conditional variance.**  $Y_i = \beta X_i + \epsilon_i, i = 1, \dots, n$ , where  $\beta = 1$  and  $\epsilon_i \stackrel{iid}{\sim} \mathcal{N}(0, 0.01)$ .

Method	Simulation 4			Simulation 5		
	$\mathbb{E}(Y   \mathbf{X})$	$\text{sd}(Y   \mathbf{X})$	Cov (Width)	$\mathbb{E}(Y   \mathbf{X})$	$\text{sd}(Y   \mathbf{X})$	Cov (Width)
PGQR ( $\alpha = 1$ )	0.15	0.07	0.95 (4.33)	0.004	<b>0.0001</b>	0.93 (0.42)
PGQR ( $\alpha = 5$ )	<b>0.14</b>	0.08	<b>0.96 (4.50)</b>	0.005	0.03	<b>0.99 (1.01)</b>
GCDS	0.23	0.05	0.87 (3.39)	<b>0.002</b>	0.0011	0.73 (0.27)
deep-GCDS	0.43	0.20	0.76 (2.88)	0.004	0.0022	<b>0.99 (0.56)</b>
WGCS	0.92	0.15	0.79 (4.41)	0.640	0.2372	0.70 (1.15)
FlexCoDE-NNR	0.23	0.003	0.92 (3.82)	0.069	0.0168	0.89 (0.27)
FlexCoDE-SAM	0.23	<b>0.002</b>	0.93 (3.83)	0.043	0.0130	0.93 (4.04)
FlexZBoost	0.45	0.06	0.82 (3.50)	1.244	0.2824	0.81 (4.13)
RFCDE	0.24	0.003	0.94 (3.97)	0.067	0.0292	0.92 (3.97)

Table 3: Table reporting the PMSE for the conditional expectation and standard deviation, as well as the coverage rate (Cov) and average width of the 95% prediction intervals, for Simulations 4 and 5. Results were averaged across 20 replicates.

The results from these two simulations averaged across 20 replicates are shown below in Table 3. The average PMSE for the  $\tau$ -th quantile levels  $Q_{Y|\mathbf{X}}(\tau)$ ,  $\tau \in \{0.1, 0.2, 0.3, 0.4, 0.5, 0.6, 0.7, 0.8, 0.9\}$  are plotted in Figure 10.

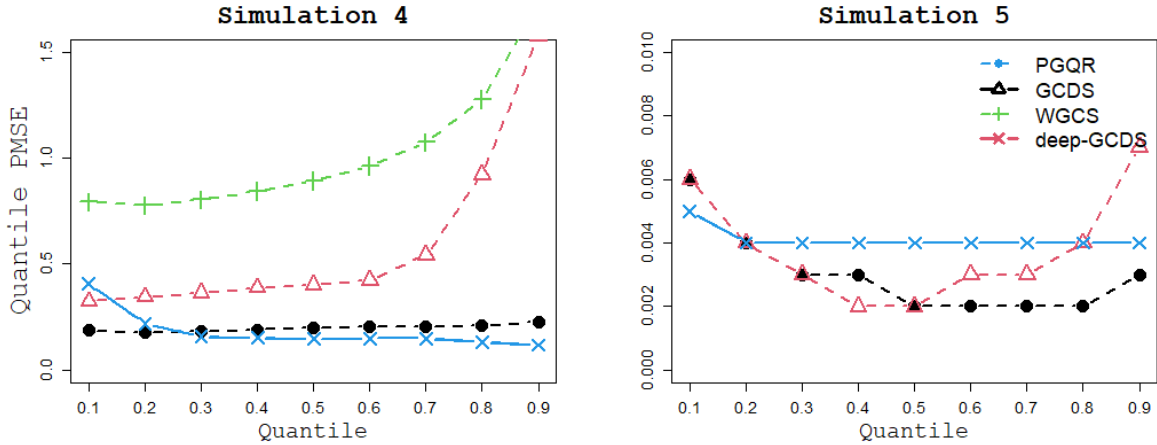


Figure 10: Plot of the average PMSE across 20 replicates for the  $\tau$ -th quantiles  $Q_{Y|\mathbf{X}}(\tau)$ ,  $\tau \in \{0.1, 0.2, 0.3, 0.4, 0.5, 0.6, 0.7, 0.8, 0.9\}$  for Simulations 4 and 5. In Simulation 5, the PMSE for WGCS is not displayed, as it lies outside of the plot area (i.e. the average PMSE for WGCS is much larger than that of the other methods).

One may be concerned whether the regularized PGQR overestimates the conditional variance when the true conditional density has a very *small* variance. To illustrate the flexibility of PGQR, Figure 11 plots the estimated conditional densities for three test observations from one replication of Simulation 5. Recall that in Simulation 5, the true conditional variance is very small ( $\sigma^2 = 0.01$ ). With the optimal  $\lambda^*$  selected using the method introduced in Section 5.2, Figure 11 shows that the estimated PGQR conditional density *still* manages to capture the Gaussian shape while matching

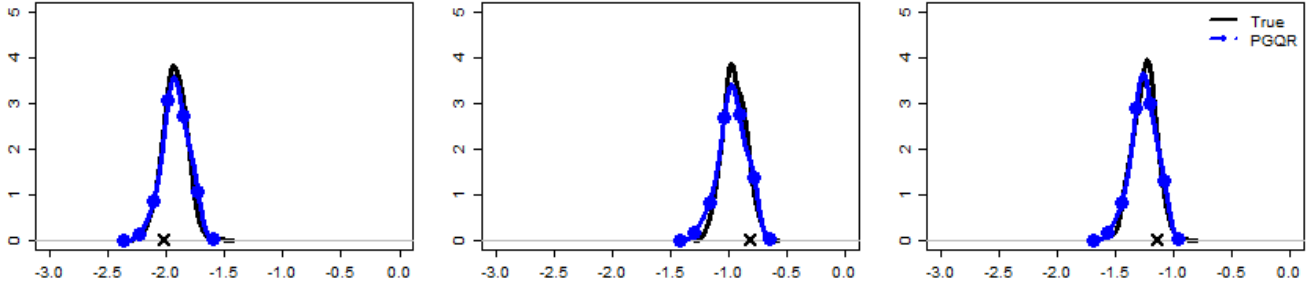


Figure 11: Plots of the estimated PGQR ( $\alpha = 1$ ) conditional densities for three different test observations in Simulation 5. The optimal  $\lambda^*$  is chosen by our tuning parameter selection method in Section 5.2.

the true variance of 0.01. If the true conditional variance is very small (as in Simulation 5), then PGQR selects a tiny  $\lambda^* \approx 0$ . In this scenario, PGQR only applies a small amount of variability penalization and thus does not overestimate the variance.

## B.2 Additional Figures

Here, we provide additional figures from one replication each of Simulations 1, 2, and 4 (with  $\alpha = 1$  in PGQR). Figures 12-14 illustrate that PGQR (blue solid line with filled circles) is better able to estimate the true conditional densities (solid black line) than GCDS, WGCS, and deep-GCDS (dashed lines). In particular, PGQR does a better job of capturing critical aspects of the true conditional distributions such as multimodality, heteroscedasticity, and skewness.

- **Simulation 1: Multimodal and heteroscedastic.**

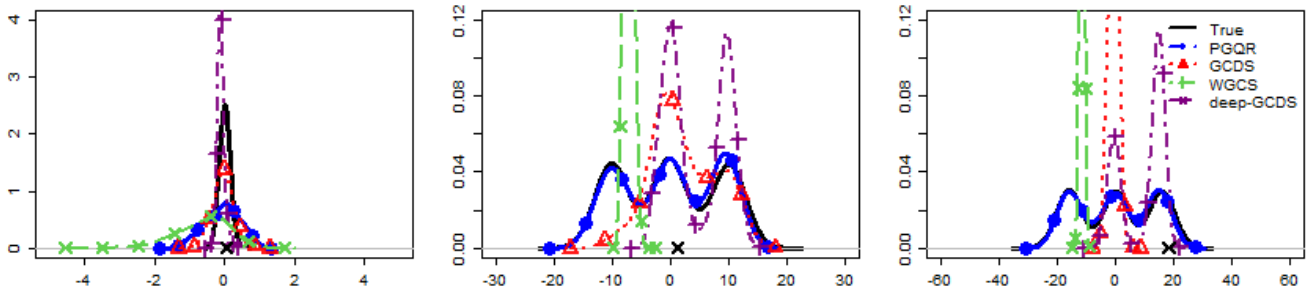


Figure 12: Plots of the estimated conditional densities of  $p(Y | \mathbf{X}_{\text{test}})$  for three different test observations from one replication of Simulation 1.

- **Simulation 2: Mixture of left-skewed and right-skewed.**

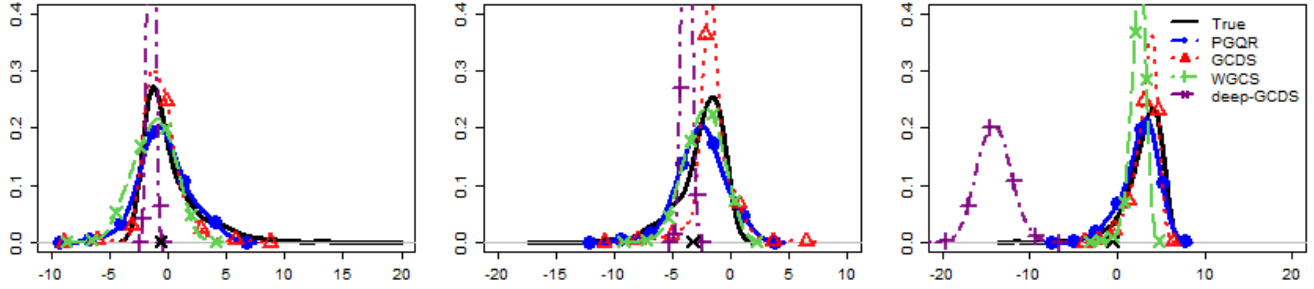


Figure 13: Plots of the estimated conditional densities of  $p(Y | \mathbf{X}_{\text{test}})$  for three different test observations from one replication of Simulation 2.

- **Simulation 4: Nonlinear function with an interaction term and one irrelevant covariate.**

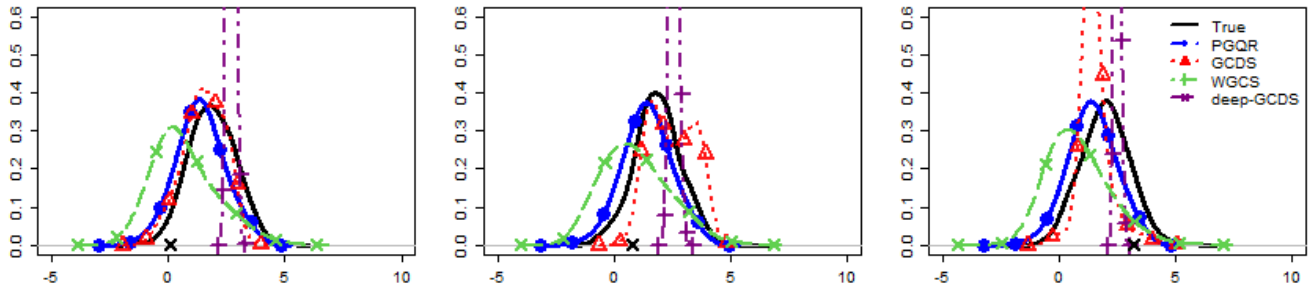


Figure 14: Plots of the estimated conditional densities of  $p(Y | \mathbf{X}_{\text{test}})$  for three different test observations from one replication of Simulation 4.

## C Sensitivity Analysis of PGQR to the Choice of $\alpha$

As mentioned in Section 3.2 of the main manuscript, we choose to fix  $\alpha > 0$  in the variability penalty (5). The main purpose of  $\alpha$  is to ensure that the logarithmic term in the penalty is always well-defined.

In this section, we conduct a sensitivity analysis to the choice of  $\alpha$ . To do this, we generated data using the same settings from Simulations 1 through 5. We then fit the PGQR model with five different choices for  $\alpha \in \{0.5, 1, 5, 10, 50\}$  and evaluated the performance of these five PGQR models on out-of-sample test data. Table 4 shows the results from our sensitivity analysis averaged across 20 replicates.

We found that in Simulations 1 through 4, PGQR was not particularly sensitive to the choice of  $\alpha$ . PGQR was somewhat more sensitive to the choice of  $\alpha$  in Simulation 5 (i.e. when the true conditional variance is very small), with larger values of  $\alpha$  leading to higher PMSE for the conditional expectation and conditional standard deviation. In practice, we recommend fixing  $\alpha = 1$  as the default  $\alpha$  for PGQR to perform well. This choice of  $\alpha = 1$  leads to good empirical performance across many different scenarios.



$\alpha$	Simulation 1			Simulation 2			Simulation 3			Simulation 4			Simulation 5		
	$\mathbb{E}(Y   \mathbf{X})$	$\text{sd}(Y   \mathbf{X})$	Cov (Width)	$\mathbb{E}(Y   \mathbf{X})$	$\text{sd}(Y   \mathbf{X})$	Cov (Width)	$\mathbb{E}(Y   \mathbf{X})$	$\text{sd}(Y   \mathbf{X})$	Cov (Width)	$\mathbb{E}(Y   \mathbf{X})$	$\text{sd}(Y   \mathbf{X})$	Cov (Width)	$\mathbb{E}(Y   \mathbf{X})$	$\text{sd}(Y   \mathbf{X})$	Cov (Width)
0.5	0.39	0.41	0.95 (23.60)	0.43	0.18	0.91 (7.69)	0.36	0.09	0.89 (5.93)	0.14	0.01	0.96 (3.95)	0.004	0.0001	0.92 (0.38)
1	0.42	0.34	0.95 (23.49)	0.38	0.11	0.93 (8.14)	0.30	0.09	0.92 (6.61)	0.15	0.07	0.95 (4.33)	0.004	0.0001	0.93 (0.42)
5	0.36	0.31	0.95 (23.41)	0.31	0.07	0.94 (8.83)	0.25	0.06	0.96 (6.60)	0.14	0.08	0.96 (4.50)	0.005	0.03	0.99 (1.01)
10	0.32	0.30	0.95 (23.40)	0.29	0.06	0.95 (9.02)	0.25	0.07	0.95 (6.55)	0.13	0.08	0.95 (4.39)	0.007	0.06	0.99 (1.33)
50	0.33	0.34	0.97 (24.15)	0.29	0.07	0.95 (9.15)	0.25	0.06	0.95 (6.63)	0.15	0.14	0.94 (4.42)	0.009	0.101	0.99 (1.81)

Table 4: PGQR results with different choices of  $\alpha \in \{0.5, 1.0, 5.0, 10.0, 50.0\}$  in the variability penalty for Simulations 1 through 5. This table reports the average PMSE for the conditional expectation and standard deviation, as well as the coverage rate (Cov) and the average width of the 95% prediction intervals. Results were averaged across 20 replicates.